



## Flank margin caves as proxies for the evolution of Cozumel Island, Mexico

Hugo E. Salgado-Garrido<sup>1,2</sup>, Salvador Trejo-Pelayo<sup>2</sup>, Elizabeth Solleiro-Rebolledo<sup>2</sup>, Peter Sprouse<sup>3</sup>, Luis M. Mejía-Ortiz<sup>4</sup>, Germán Yáñez<sup>5</sup>, and Rafael López-Martínez<sup>2\*</sup>

<sup>1</sup> Posgrado en Ciencias de la Tierra, Universidad Nacional Autónoma de México, Circuito de los Posgrados s/n Ciudad Universitaria, Coyoacán, Mexico City, 04510, Mexico.

<sup>2</sup> Laboratorio de Carbonatos y Procesos Kársticos. Instituto de Geología, Universidad Nacional Autónoma de México, Av. Universidad 3000, Coyoacán, Mexico City, 04510, Mexico.

<sup>3</sup> Zara Environmental LLC. 2104 Hunter Road San Marcos Texas 78666, United States of America.

<sup>4</sup> Laboratorio de Carcinología y Bioespeleología, División de Desarrollo Sustentable, Universidad de Quintana Roo, Av. Andrés Quintana Roo s/n, Cozumel 77600, Quintana Roo, Mexico.

<sup>5</sup> Círculo Espeleológico del Mayab A.C. Av. 60 No. 17, Col. 10 de abril, Isla Cozumel, Quintana Roo, 77600, Mexico.

\*Corresponding author (R. López-Martínez): [ralopezm@geologia.unam.mx](mailto:ralopezm@geologia.unam.mx)

### EDITORS:

Angel Francisco Nieto-Samaniego  
Luigi A. Solari

### HOW TO CITE:

Salgado-Garrido H. E., Trejo-Pelayo, S., Solleiro-Rebolledo, E., Sprouse, P., Mejía-Ortiz, L. M., Yáñez, G., & López-Martínez R. (2024). Flank margin caves as proxies for the evolution of Cozumel Island, Mexico. *Revista Mexicana de Ciencias Geológicas*, 41(3), 189–205. DOI: <http://dx.doi.org/10.22201/igc.20072902e.2024.3.1796>

Manuscript received: April 17, 2024  
Corrected manuscript received: July 24, 2024  
Manuscript accepted: July 25, 2024  
Published Online: December 1, 2024

### COPYRIGHT

© 2024 The Author(s).  
This is an open-access article published and distributed by the Universidad Nacional Autónoma de México under the terms of a [Creative Commons Attribution 4.0 International License \(CC BY\)](https://creativecommons.org/licenses/by/4.0/) which permits unrestricted use, distribution, and reproduction in any medium, provided the original author and source are credited.



### ABSTRACT

There has been a recent increase in research on coastal karst, revealing numerous morphologies connected to the relative sea-level position. In particular, the flank margin caves are recognized as excellent markers of ancient sea-level changes and paleo-coast lines. Here, we characterized the Cozumel flank margin caves using cave morphology and morphometry, surface terrace maps, and host rock microfacies. The Cozumel flank margin caves exhibit three main morphologies: classic, multiphase, and banana hole. Microfacies analysis reveals that classical and multiphase flank margin caves morphologies evolved in rocks formed in a protected lagoon environment. In contrast, banana hole morphologies developed in rocks belonging to a margin platform and sand shoal environment. Morphometric values reveal high erosion or diagenetic overprint, particularly in banana hole morphologies. The distribution of flank margin caves in Cozumel, located on terraces II and III, is closely linked to the last highstand sea level MIS 5e, indicating the past sea-level position and revealing changes in the island landscape, starting as a cluster of small sandy islands merging into a single island subsequently. The development of Cozumel flank margin caves and sedimentary units is comparable to other carbonate islands. However, differences in the size of Cozumel flank margin caves compared to The Bahamas analogs open a new window to additional studies about the time needed for cave development.

Key words: flank margin caves; isolated carbonate platform; microfacies; cave morphometry; cave morphology.

### RESUMEN

Recientemente ha aumentado la investigación sobre el karst costero, revelando numerosas morfologías relacionadas con la posición relativa del nivel del mar. En particular, las cuevas de flanco de margen son reconocidas como excelentes marcadores de antiguos cambios en el nivel del mar y paleo-líneas de costa. En el presente trabajo, caracterizamos las cuevas de flanco de margen de Cozumel utilizando morfología y morfometría de cuevas, mapas de terrazas superficiales y microfacies de la

*roca de caja. Las cuevas de flanco de margen de Cozumel exhiben tres morfologías principales: clásica, multifásica y banana hole. El análisis de microfacies revela que las morfologías clásicas y multifásicas evolucionaron en rocas formadas en un ambiente de laguna protegida, mientras que las banana hole lo hicieron en rocas pertenecientes a un ambiente de margen de plataforma y bancos de arena. Los valores morfométricos revelan un alto grado de erosión o sobreimpresión diagenética, particularmente en las morfologías banana hole. La distribución de las cuevas de flanco de margen en Cozumel, situadas en las terrazas II y III, está estrechamente relacionada con el último cortejo transgresivo alto MIS 5e, lo que indica la posición antigua del nivel del mar y revela cambios en el paisaje de la isla, que comenzó como un grupo de pequeñas islas arenosas que se fusionaron posteriormente en una sola isla. El desarrollo de las cuevas de flanco de margen y unidades sedimentarias de Cozumel es comparable con otras islas carbonatadas. Sin embargo, la diferencia en el tamaño de las cuevas de flanco de margen de Cozumel, en comparación con sus análogos de Las Bahamas, abre una nueva ventana a estudios adicionales sobre el tiempo necesario para la génesis de estas cuevas.*

*Palabras clave: cuevas de flanco de margen; plataforma carbonatada aislada; microfacies; morfometría de cuevas; morfología de cuevas.*

## INTRODUCTION

In the coastal systems, karst features are triggered by the sea-level position (Carew and Mylroie, 1995; Mylroie and Carew, 1995b; Mylroie and Mylroie, 2007; de Waele *et al.*, 2009; van Hengstum *et al.*, 2011, 2015). These environments are among the most critical coastal landscapes where the dissolution, precipitation, and sedimentation processes are self-regulated in response to sea level change, leaving geomorphological and sedimentary evidence of sea level variations, particularly in flank margin caves (Mylroie & Mylroie, 2017a; van Hengstum *et al.*, 2011, 2015).

The flank margin caves (FMCs) are large solution voids in the contact zone between fresh and marine groundwater, triggered by mixing solution and complex geochemical processes related to organic matter oxidation. The mixing solution occurs at the top and the bottom of the freshwater lens on the flanks of the landmass; their position at the edge of the lens allows the superposition of the vadose-phreatic mixing zone on the top of the freshwater-sea water mixing zone (Carew & Mylroie, 1995; Mylroie & Carew, 1990, 1995a, b; Mylroie & Mylroie, 2007; Roth *et al.*, 2006; van Hengstum *et al.*, 2015). In some islands, authors recognized the need for a minimum 10 to 40 km radius of the emerged area to install a freshwater lens capable of generating flank margin caves (Larson & Mylroie, 2018).

The FMCs are considered hypogenic caves and are accessible through weathering, collapse, or dissolution structures that intercept them (Mylroie & Mylroie, 2017a; Palmer, 1991). Their morphologies are isolated or fused phreatic chambers parallel to the coast, exhibit spongiform and ramiform patterns, curvilinear walls, blind passages, globular rooms, which are limited vertical extension, flat roofs with cupolas, pendant structures, and residual bedrock pillars; also, lack of real conduits, flow structures, and fluvial sediments is notable (Mylroie & Carew, 1990, 1995a; Mylroie & Mylroie, 2007, 2017a; Palmer, 1991). A subtype of FMC is a banana hole that shows similar features in small and simple caves, formed in a prograding environment considered stillstand morphologies and an example of syndepositional caves (Mylroie & Mylroie, 2017a).

The FMC model suggests that large FMC morphologies appear very quickly, near to 10 ky (Mylroie, 2013; Mylroie & Carew, 1990, 1995a, 1995b; Mylroie & Mylroie, 2017a). In comparison, the banana hole morphologies occur faster (Mylroie *et al.*, 2016; Mylroie & Mylroie, 2017a).

FMC development is linked to freshwater lens position triggered by the sea level. On the other hand, the size, complexity, and areal footprint depend on the stability of freshwater lens (Carew & Mylroie, 1995; Mylroie & Carew, 1990, 1995a, 1995b; Mylroie & Mylroie, 2007; Roth *et al.*, 2006). All these conditions are controlled by tectonic and glacioeustatic changes (Mylroie & Mylroie, 2007). In addition, heterogeneous epigenetic CO<sub>2</sub>, biogeochemical processes, and overprinting events increase the areal footprint (Gulley *et al.*, 2013; 2015; 2016; Mylroie *et al.*, 2020; Breithaupt *et al.*, 2021a). Finally, despite being affected by karst denudation, which reduces the size of sedimentary records (corals, sediments and host rock caves), they can retain the sea-level position signal (Mylroie & Mylroie, 2017b).

The previous properties highlight that FMCs provide an excellent tool for determining ancient sea level, especially in environments without neotectonic activity and considered extraordinary proxies for the determination of the sea-level position during the last highstand at six meters above sea level (m a.s.l.) in The Bahamas archipelago (Carew & Mylroie, 1995; Mylroie & Carew, 1990; 1995a, 1995b; Mylroie & Mylroie, 2007; van Hengstum *et al.*, 2015).

Yucatan Peninsula hosts a massive karst aquifer with the most extensive underwater cave system, a large number of dolines locally called cenotes, as well as complex dry cave systems (Bauer-Gottwein *et al.*, 2011; Beddows *et al.*, 2007a, 2007b, Kambesis & Coke IV, 2013; Smart *et al.*, 2002, 2006). The extensive exploration of the area reports 1679.4 km of subaquatic caves and 359.7 km of subaerial caves (QRSS, 2023). However, despite considerable research on the previous morphologies, their speleogenesis and direct relationship with ancient sea-level positions are still unclear. Alternatively, some authors recognized the presence of FMCs caves (Kambesis & Coke IV, 2013; Kelley *et al.*, 2006), but there are no studies about its development and relationship with sea level changes.

In this way, the present work sheds new light on the characterization of flank margin caves and their use as an excellent proxy of sea level during the Late Pleistocene in the Mexican Caribbean region.

## GEOLOGICAL SETTING

The Yucatan platform in southeast Mexico comprises a submerged and an emerged region, with a total extent of 300000 km<sup>2</sup>

(Bauer-Gottwein *et al.*, 2011). The emerged portion, including the adjacent islands, is recognized as the Yucatan Peninsula (Figure 1a), with an area of 39340 km<sup>2</sup> (Frausto-Martínez *et al.*, 2019).

Yucatan Peninsula (YP) is a carbonate platform composed of more than 3000 m thick limestone sequence (López-Ramos, 1973), including eogenetic limestone (Choquette & Pray 1970; Kambesis & Coke IV, 2013; Smart *et al.*, 2002, 2006), considered one of the typical karstic landscapes (Lugo-Hubp *et al.*, 1992). The Mexican Geological Survey (SGM) recognized limestones in the central region with ages ranging from Paleocene to Pliocene and Quaternary younger deposits towards the coastal areas (SGM, 2006; Ward, 1997).

The Carrillo Puerto Formation is the most exposed in the YP (SGM, 2006), deposited between the Miocene and Pliocene (Butterlin & Bonet, 1963). This formation is overlaid by Pleistocene and Holocene carbonate sandstones, corresponding to the deposits

of contemporary beaches (Ward, 1997; Ward & Brady, 1979). Some authors argued that the YP is tectonically stable (Beddows *et al.*, 2007a, b; Blanchon *et al.*, 2009; Moseley *et al.*, 2013, 2015; Smart *et al.*, 2002, 2006) at least since the Late Pleistocene with a slow subsidence rate of ~1 mm·ky<sup>-1</sup> (Emery & Uchupi, 1972).

### Cozumel Island

Cozumel is located northeast of the YP in Quintana Roo state, Mexico, located between 20°16'12"N and 20°35'15"N latitude and between 87°01'48"W and 86°43'48"W longitude (Figure 1b) (Mejía-Ortiz *et al.*, 2007). The island shares a geological evolution with the YP, controlled mainly by sea level changes (Ward, 1997; Salgado-Garrido *et al.*, 2022).

The Cozumel Island is a small, low-lying island that belongs to a series of isolated carbonate platforms extending from Belize to the northeast of the YP (Gischler & Lomando, 1999, 2000). The island emerges over a horst located in the footwall of a major normal fault, developed along the continental margin with northeasterly trends (Uchupi, 1973; Ward, 1997), close to the trend of a tilted fault block in Belize (Dillon & Vedder, 1973) and NNE-SSW lineaments in the YP interior (Smart *et al.*, 2006). This normal faulting is related to the Yucatan Basin aperture, initiating from the Cretaceous to the Paleogene (Dillon & Vedder, 1973; Rosencrantz, 1990), suggesting the time when the Cozumel Island separated from the mainland.

Nowadays, Cozumel Island is the largest carbonate island in Mexico (Frontana-Urbe & Solis-Weiss, 2011) with an area of 482 km<sup>2</sup> (Mejía-Ortiz *et al.*, 2007), has an average altitude of 5 m a.s.l. while the highest elevation is 16 m a.s.l. towards the island center (INEGI, 2020a). The island is surrounded by deep water, 400 m deep on the west side by the Cozumel channel, while to the east, depths reach around 1000 m (Athie *et al.*, 2011). The island climate is hot and humid, with plentiful rainfall in the summer, an average precipitation of 1,504 mm/yr, and an average temperature of 25.5 °C (Frausto-Martínez *et al.*, 2019). The nearest data indicate that evaporation is greater than annual rainfall (Cabadas-Báez *et al.*, 2010).

The upper Cozumel Island displays two lithostratigraphic units separated by caliche layers (Figure 2). The first unit (Unit 1) is a well-consolidated limestone belonging to the Carrillo Puerto Formation, covered by friable Late Pleistocene carbonate sandstones (Unit 2) deposited during the last highstand sea level or Marine Isotopic Stage (MIS) 5e (Salgado-Garrido *et al.*, 2022). Carbonate sands were deposited from subtidal and supratidal environments. The upper and lower limits of carbonate sands are bounded by pedogenic carbonates layers (Figure 2), associated with the latest lowstand sea levels as MIS 4 and MIS 6 (Valera-Fernández *et al.*, 2020; Salgado-Garrido *et al.*, 2022). Also, Holocene sediments accumulate on the coasts (Ward, 1997).

Salgado-Garrido *et al.* (2022) recently proposed a facies map and three morphostratigraphic units controlled by glacioeustatic changes corresponding to terrace I or flat terrains from 1 to 4 m a.s.l., terrace II or flat terrains with ancient beach ridge progradation from 4 to 6 m a.s.l., and terrace III consistent to highest zones from 7 to 16 m a.s.l. developed during the last highstand sea level. During the subsequent lowstand sea level, caliche 2 begins to form.

The Cozumel Island displays many karst features, including the wave, splash, and spray marine zones *e.g.*, sea caves and karrenfields mixed with biokarst among others. Also, tafoni and littoral inlet morphologies are documented (Figure 1). All these karst features decrease in abundance toward the center of the island, where dissolution structures such as cenotes and solution pans, locally named "aguadas" or "rejoyadas", are most evident and even increase in size (Mejía-Ortiz *et al.*, 2007).

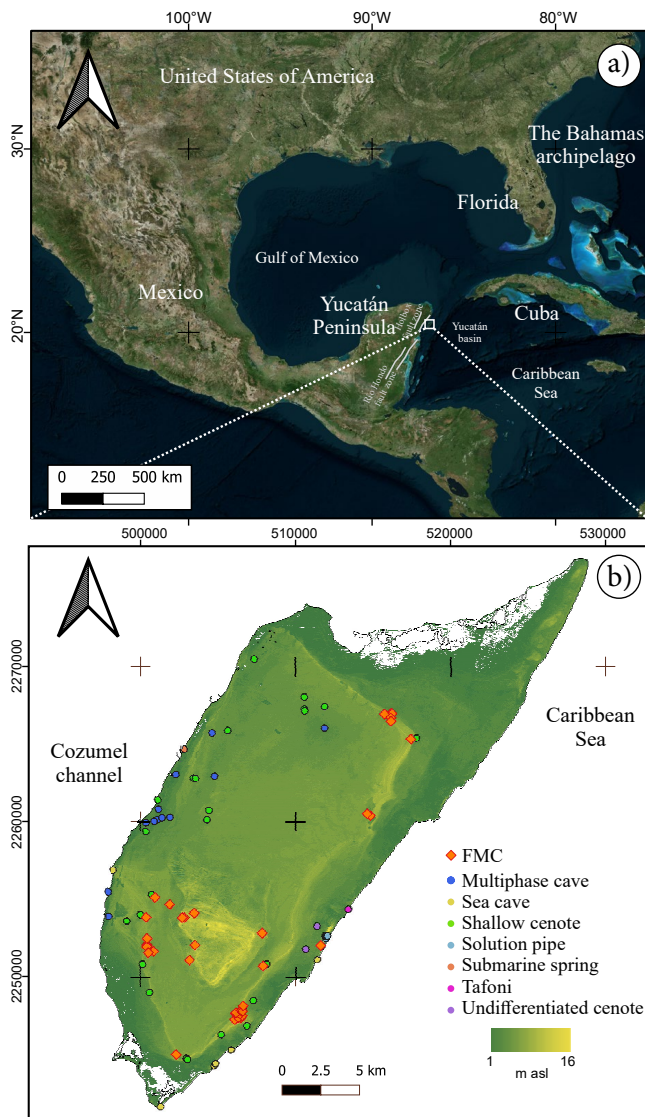


Figure 1. Location map. a) The Yucatan Peninsula in southeastern Mexico, geographic coordinates. b) Digital elevation model of Cozumel Island (INEGI, 2020a, 2020b) with different cave entrances, UTM coordinates 16N. Orange diamonds represent all flank margin caves (FMC) of terraces I and II in our cave inventory. The color circles represent a different speleogenesis according to the main characteristics in Supplementary Table 1. Meters above sea level (m a.s.l.).

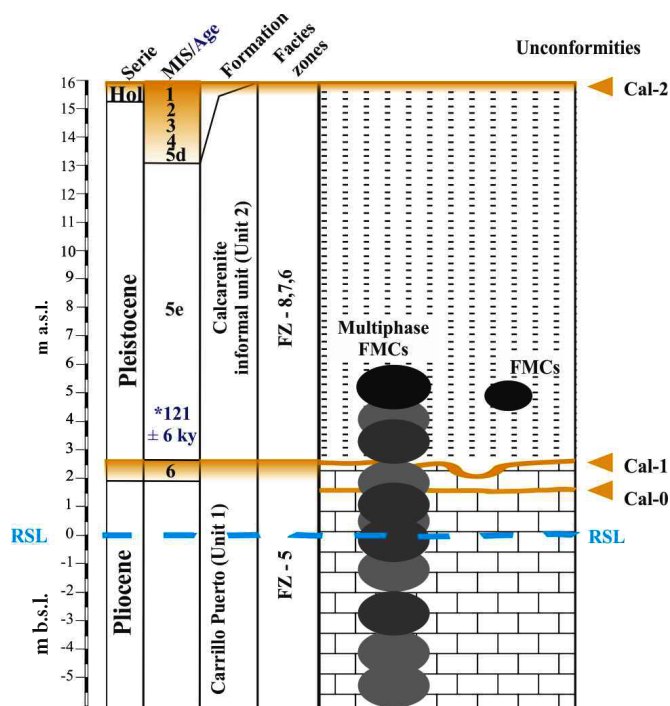


Figure 2. Synthetic lithostratigraphic column of Cozumel Island based on Salgado-Garrido *et al.* (2022). The black ellipse indicates the FMC position during MIS 5e, and the stacked grey ellipses correspond to multiphase events. The maximum height of deposits represents the current height of the ancient central cay (16 m a.s.l.). \* Coral age from Szabo *et al.* (1978). Current relative sea level (RSL), meters above sea level (m a.s.l.), meters below sea level (m b.s.l.), caliche (Cal), marine isotopic stage (MIS), Holocene (Hol) and facies zone (FZ) identified on the island based on Wilson model.

## METHODOLOGY

### Cave morphology and data

We compiled a total of 98 cave entrances based on available databases, including dry caves, cenotes, sea caves, and cave systems (QRSS, 2023), plus new records for six isolated dry caves and one cenote from field surveys called Murcielagos BH, Cantera Transversal, and Nohoch Hool, Kana Nah, El Lina, Chichan Nah, and cenote Chenchón (Figure 1b and Supplementary Table 1).

Garmin Etrex, 30 GPS with a Garmin GPS 17X HVS (NMEA 0183) antenna, was used to georeference new cave entrances with an accuracy of  $\pm 3$  m. For the cave survey, a Leica DistoX310 laser distance meter was used with the standard cave mapping methods (Häuselmann, 2011). The distance meter calibration was carried out by acquiring 56 measurements in 14 ways with an error =  $0.5^\circ$ , following the DistoX2 calibration manual of Paperless Cave Surveying (Heeb, 2013). All cave entrances were georeferenced using ArcGIS 10.1 and QGIS 3.4.15 software. The flank margin cave morphologies were described according to Mylroie and Carew (1990; 1995a, 1995b), Mylroie and Mylroie (2007; 2017a), and Palmer (1991).

### Host rock microfacies analysis

Cave wall samples were selected to corroborate the host rock depositional environment and field survey information. Thin sections of  $30 \mu\text{m}$  were prepared and analyzed directly under a petrographic microscope Olympus model BX51. Photomicrographs were taken using the Image-Pro Plus v.5.1.1 software. The carbonate classification and microfacies descriptions were done following the criteria of Dunham (1962), modified by Embry and Klovan (1971) to assign

the Standard Microfacies (SMF) and the Facies Zones (FZ) based on Flügel (2010).

### Cave morphometric analysis

Morphometric analysis was carried out using eighteen available cave surveys. Eleven previous and seven new topographies were used. For the latter, data acquisition consisted of establishing topographic stations from which radial measurements were taken to obtain cave contours. Topodroid 5.1.40 software and an Android cell phone were used for drawing surveys. Afterward, surveys were exported and processed using the software ImageJ IJ1.46r from the National Institute of Health (NIH).

Morphometric interpretation followed the criteria established by Lace (2008) and Waterstrat *et al.* (2010) with measurements of the following parameters: perimeter (P), area (A), maximum entrance width (EW), maximum internal width (IW), and the ratios A/P, EW/IW, and the axis short/axis long (AS/AL) of a rectangle shape over the cave area.

### Surface terrace map and paleo island emerged areas

The terrace map represents the area that has emerged. The terrace map was based on altimetry and field evidence, combined with landforms and microfacial interpretations of the rocks exposed on the island, correlating to the contemporary landscape.

The altimetric changes include high-resolution elevation models (26 pieces) data using terrain data collected with a LiDAR sensor at 5 m pixels and 1 m for vertical resolution. These data were collected in 2008 and adjusted by the Instituto Nacional de Estadística y Geografía (INEGI) using the ITRF92 Epoch 1988.0 for the horizontal datum and NAVD88 for the altitude (INEGI, 2020a, 2020b). All maps were constructed and corrected using GIS ArcGIS 10.1 and QGIS 3.4.15 software.

To establish the paleo island emerged areas, we took the geological information of Salgado-Garrido *et al.* (2022), the maximum sea-level position during the last highstand MIS 5e of +6 m a.s.l. (Blanchon *et al.*, 2009), and the surface terraces map. These values were also compared with parameters proposed by Larson and Mylroie (2018) and processed with ImageJ IJ1.46r.

## RESULTS

### Flank margin cave morphologies

Forty-two caves are interpreted as FMCs based on their island morphology and distribution (Table 1). The rest of the caves correspond to cenotes with minimal or no vadose zone, horizontal and deep long development, and marine caves (Supplementary Table S1). The FMCs are located towards the island's center and above current sea level on the flanks of terraces II and III, mainly on ancient beach ridge progradations (Figures 3a–3f). All FMCs are isolated and scattered caves on the island with evidence of phreatic passages or chambers without significant horizontal development and flow evidence, occurring at a height of 3–6 m a.s.l. (Figure 3). The cave entrances are semicircular, with variable widths and vadose zones associated with debris cones at the center or reaching the water table. The height of the phreatic globular chambers is restricted between 1–6 m. We divided the FMCs into three evident morphologies as follows.

### Multiphase-Flank Margin Caves

Multiphase-FMCs morphologies (Figure 3) exhibit a vadose and underwater (phreatic) zone. They appear in the innermost part of the island at the flanks of the ancient central cay (Salgado-Garrido *et al.*, 2022), represented by Chempita, Chenchón, and Chechen Ha cenotes.

Table 1. Cozumel Flank margin caves inventory. Abbreviations: BH= banana hole. FT= flat terrains. ABR= Ancient beach ridge. ANI= ancient narrow island. AICE= ancient isolated cays of the east. ACC= ancient central cay. Host rock facies zone refers to Wilson model from Flugel (2010). Reference data (a) Sprouse, 2020. (b) Mejía-Ortíz *et al.*, 2007. (c) This paper.

Register number	Cave name	Subtype cave	Island region	Landform	Terrace entrance	Host rock facies zone
1	San Gervasio 1 <sup>a</sup>	BH	Northeast, San Gervasio area	FT and ABR	II	7
2	San Gervasio 2 <sup>a</sup>	BH	Northeast, San Gervasio area	FT and ABR	II	7
3	Palma secuestrada <sup>a</sup>	BH	Center, Cedral area	FT and ABR	II	7
4	Palmar <sup>a</sup>	BH	Center, Cedral area	FT and ABR	II	7
5	Ferchango <sup>a</sup>	BH	Center, Cedral area	FT and ABR	II	7
6	Aktun Balam <sup>c</sup>	BH	Center, Cedral area	FT and ABR	II	7
7	Cedral track <sup>c</sup>	BH	Center, Cedral area	FT and ABR	II	7
8	Cueva de los Murciélagos <sup>a</sup>	BH	Center, Cedral area	FT and ABR	II	7
9	San German <sup>a</sup>	BH	Center, Cedral area	FT and ABR	II	7
10	San Gabriel <sup>a</sup>	BH	Center, Cedral area	FT and ABR	II	7
11	Ramon <sup>a</sup>	BH	East, Buenavista area	ANI	III	6, 7
12	Mosquito <sup>a</sup>	BH	East, Buenavista area	ANI	III	6, 7
13	Andale 1 <sup>a</sup>	BH	East coast	AICE	III	6, 7
14	Andale 2 <sup>a</sup>	BH	East coast	AICE	III	6, 7
15	Escondida <sup>a</sup>	BH	Center, Cedral area	FT and ABR	II	7
16	Magnolia <sup>a</sup>	BH	East, Buenavista area	ANI	III	6, 7
17	Buenavista <sup>a</sup>	BH	East, Buenavista area	ANI	III	6, 8
18	Nohoch Hool <sup>c</sup>	Classic	Island center	ACC	III	5, 7, 8
19	Murcielagos BH <sup>c</sup>	BH	Northeast	ANI	III	6, 7
20	Cantera Transversal <sup>c</sup>	BH	Northeast	ANI	III	6, 7
21	Piramide <sup>a</sup>	BH	East, Buenavista area	ANI	III	6, 7
22	Chaac Mool <sup>a</sup>	BH	East, Buenavista area	ANI	III	6, 7
23	Kana Nah <sup>c</sup>	BH	Northeast, San Gervasio area	ANI	III	6, 7
24	El Lina <sup>c</sup>	BH	Northeast, San Gervasio area	ANI	III	6, 7
25	Chichan Nah <sup>c</sup>	BH	Northeast, San Gervasio area	ANI	III	6, 7
26	Estacionamiento San Gervasio <sup>c</sup>	BH	Northeast, San Gervasio area	ANI	III	6, 7
27	Pelovino <sup>a</sup>	BH	Northeast, San Gervasio area	ANI	III	6, 7
28	Mariposa <sup>a</sup>	Classic	Island center	ACC	III	7, 8
29	Ariadna <sup>a</sup>	Classic	Island center	ACC	III	7, 8
30	Ruinas <sup>a</sup>	BH	East, Buenavista area	ANI	III	6, 7
31	Cueva de la llanta <sup>a</sup>	BH	East, Buenavista area	ANI	III	6, 7
32	Espinosa <sup>a</sup>	BH	East, Buenavista area	ANI	III	6, 7
33	Gilberto <sup>a</sup>	BH	East, Buenavista area	ANI	III	6, 7
34	Polo <sup>a</sup>	BH	East, Buenavista area	ANI	III	6, 7
35	Cueva del Cementerio <sup>a</sup>	BH	East, Buenavista area	ANI	III	6, 7
36	Cueva del camino BH <sup>c</sup>	BH	East, Buenavista area	ANI	III	6, 7
37	Chen Chile <sup>a</sup>	BH	Center, Cedral area	FT and ABR	II	7
38	Yaxché <sup>a</sup>	BH	South	ANI	III	6, 7
39	Cenote Basurero <sup>a</sup>	Multiphase	Island center	FT and ABR	II	7
40	Cenote Chempita <sup>b</sup>	Multiphase	Island center	ACC	III	5, 7, 8
41	Cenote Chenchon <sup>c</sup>	Multiphase	Island center	ACC	III	5, 7, 8
42	Cenote Chechen Ha <sup>a</sup>	Multiphase	Island center	ACC	III	5, 7, 8

They are on terrace III, with circular to oval entrances. Usually, the upper part of the caves is covered by the caliche 2. The subaerial portion comprises 6-8 m a.s.l. of highly weathered calcarenites (Figures 4, 5a–5b).

The vadose zone displays a semi-spherical chamber. In Chempita, Chenchón and Chechen Ha cenotes, the walls contain abundant tufaceous speleothems and small globular chambers with blind passages (Figures 4, 5a–5b). The subaquatic zones have reached a depth of more than -60 m b.s.l. through sub-horizontal and sub-vertical conduits with collapse structures and scarce speleothems (Chempita and Chenchón).

### Classic Flank Margin Caves

Two types of FMCs are defined based on their distribution across the island and their morphologic features. The first occurs at the flanks of terrace III (ancient central cay), and the second in the ancient beach ridge progradation, developed between terrace II and III (Figures 3). Classic FMCs (Nohoch Hool, Ariadna, and Mariposa) are in the flanks of the ancient central cay, do not reach the water table (Figures 3, 4c), exhibit cave entrances between 7–9 m a.s.l. and height up to 5 m in their chambers. Ceilings are near the surface, bounded by a caliche 2. These caves display phreatic morphologies from lenticular to oval chambers with round, smooth walls and blind passages (Figure 6).

They also show tuffaceous speleothems in their walls and ceilings. Some pendant structures and residual bedrock pillars are present. The lack of fluvial sediments, scallops, and large debris collapses stands out.

### Banana hole Flank Margin Caves

Banana hole occurs on the ancient beach ridge progradations of terraces II and III, in the leeward areas of ancient narrow strip islands and the flat landform (Figure 3). These formations are found in the northeast (San Gervasio area, Cantera Transversal, and Murcielagos BH caves), the eastern in the Buenavista area, and westward in the Cedral area (Figures 3b–3c).

Entrances are semicircular between 5–7 m a.s.l. (Figures 4d–4f), and their ceilings are a few centimeters down the surface, delimited by the caliche 2 (Figure 7). Sometimes, there is more than one entrance, and collapse structures are frequent (Cedral and Buenavista area). Phreatic morphologies display lenticular to oval chambers with round and smooth walls. The rooms end in blind passages. The ceilings are usually flat with small cupolas (Figure 7). The chamber heights are restricted to 1 m in the Murcielagos BH and Cantera Transversal caves

(Figure 7), 2 m in the San Gervasio and Cedral area, and up to 2.5 m in Buenavista area (Figure 7). Inside the chambers, an increase in residual bedrock pillars and a notable lack of scallops, fluvial deposits, and large debris collapses are evident. Stand out the absence of speleothems. The subaerial portion of Multiphase-FMCs and FMCs morphologies in Cozumel Island coincide with the descriptions of typical FMC of Mylroie and Carew (1990, 1995a, 1995b) and Mylroie and Mylroie (2017a), and they also are consistent with the fusion of adjacent chambers to form spongiform patterns (Palmer, 1991).

### Morphometric analysis

Of 42 FMCs, only 18 FMCs were classified following Roth *et al.* (2006). We classified four FMCs into small (<100 m<sup>2</sup>), eleven into medium (100 m<sup>2</sup>–1000 m<sup>2</sup>), and three into large sizes (>1000 m<sup>2</sup>). The size of the Cozumel caves ranges between 42.7 m<sup>2</sup> (Cantera Transversal) to 1171.9 m<sup>2</sup> (Aktun Balam), reported the Cedral track case with a mean area of (536.5 m<sup>2</sup>) e.g., Magnolia, Estacionamiento San Gervasio, Palma Secuestrada, Nohoch Hool, and Chempita and Chenchón cenotes

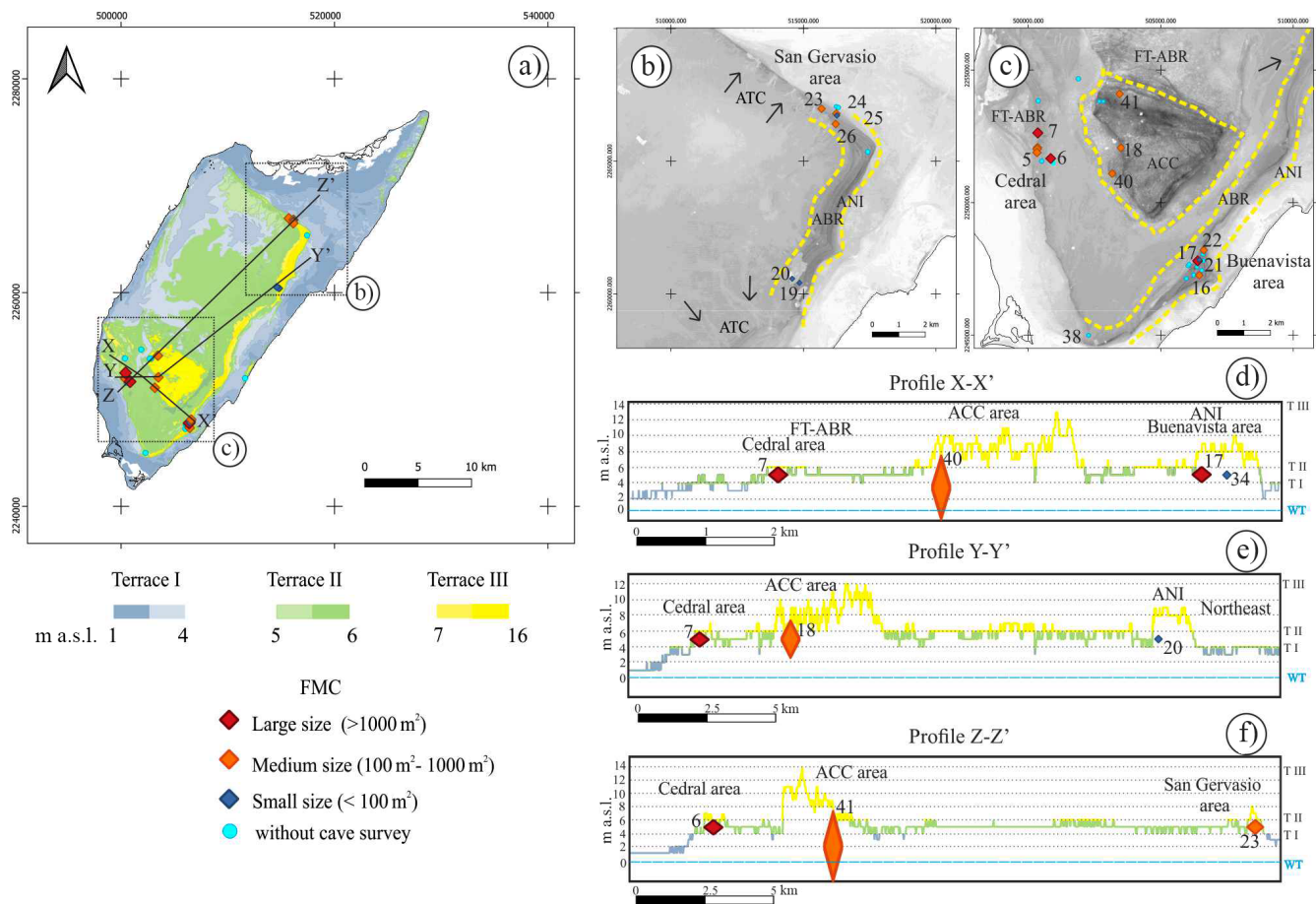


Figure 3. Terrace map and Cozumel Island features. (a) General terraces map based on Salgado-Garrido *et al.* (2022) and DEMs (INEGI, 2021a). Diamonds represent FMC; size, color, and vertical extent indicate an estimate of the footprint. Lines X, Y, and Z correspond to topographic profiles. (b) and (c) Highlight the geomorphologic features. Numbers represent the register number of Tables 1, 2 and Supplementary Table S1. (b) San Gervasio area (northeastward), with ancient tidal channel (ATC) indicated by black arrows, FMCs are present on the flanks of terrace III, ancient beach ridge progradation (ABR), and ancient narrow islands (ANI). (c) Buenavista area (northeastward), where FMC entrances are over ABR in terrace III. In the Cedral area (westward), the FMCs are developed on terrace II, over flat terrains and ancient beach ridge progradation (FT-ABR). The yellow dashed line represents the ancient Central Cay (ACC) and ANI. d–f. Topographic profiles and FMCs positions on Cozumel Island, from the general terrace map. (d) Profile X-X' is approximately W-E, from the Cedral area to the Buenavista area. (e) Y-Y' profile crosses from the Cedral area to the Cantera Transversal. (f) Z-Z' profile crosses from the Cedral area to the San Gervasio area, both profiles are approximately from S45W degrees to N45E. The colors of the profile represent the terrace to which they belong. T-I-II-III = terrace I, II, III. WT = water table.

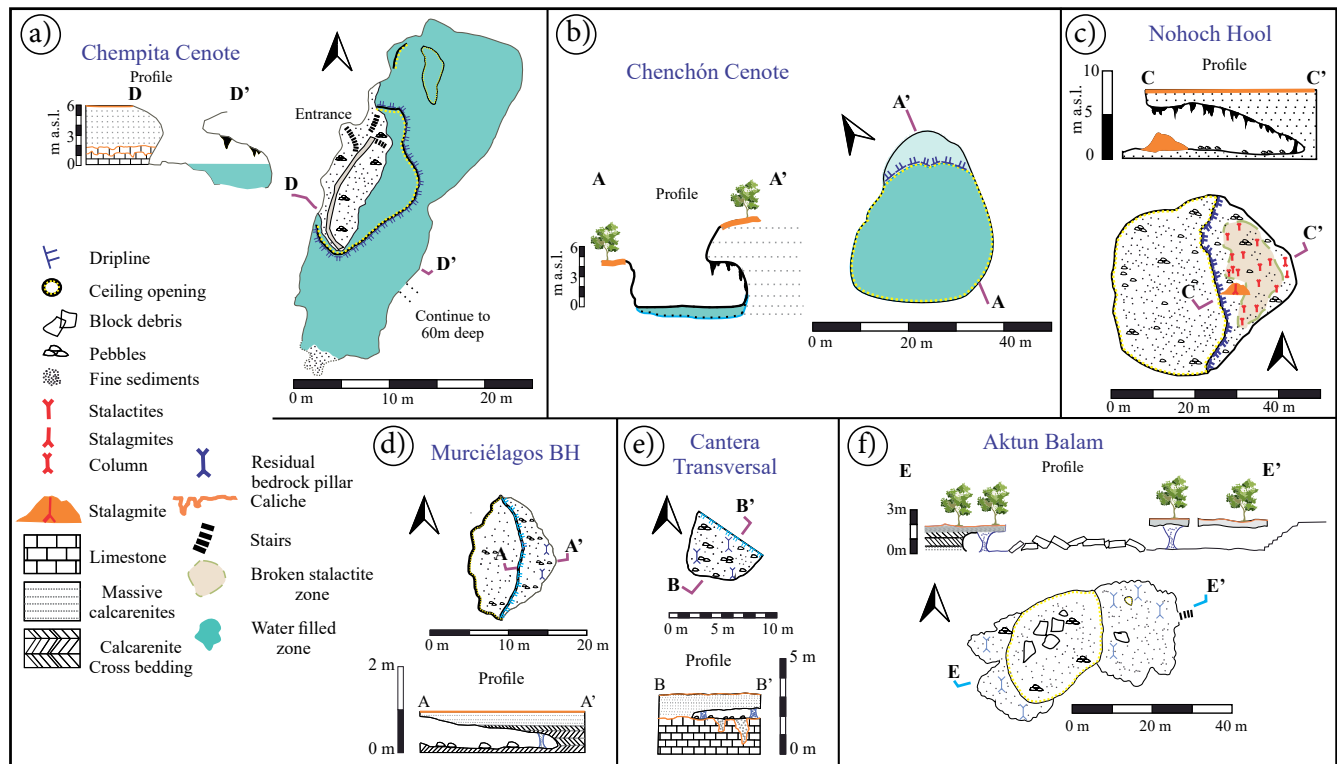


Figure 4. Flank margin cave surveys. (a–b) Multiphase FMC. (c) Classic FMC. (d–f). Banana hole FMC.

(Table 2). The A/P ratio (Table 2) varies from 1.04 (Murciélagos BH) to 6.6 (Aktun Balam), 7.16 (Chenchón cenote), and 8.01 (Cedral track).

The EW/IW ratio has similar tendencies to the A/P, ranging from 0.40 (Cenote Chempita) to 1.34 (Cantera Transversal) with a mean of 0.637 (Table 2). Also, the AS/AL ratio continues the trend of high values in this type of cave, ranging from 0.44 (Murciélagos) to 1.11 (Cantera Transversal), and 0.3 for Cedral track (Table 2). Values of A vs P (Figure 8a), show a certain linear tendency with  $R^2 = 0.858$ . In this way, A/P ratio vs. EW/IW ratio (Figure 8b) does not show a clear trend or group of caves.

#### Host rock and microfacies analysis

Salgado-Garrido *et al.* (2022, tab. 2) analyzed sixty-four cave samples, showing the lithostratigraphic features composed of the Carrillo Puerto Formation ending in caliche 1, only exposed in quarries and cenotes such as Chempita. The second unit overlaying the Carrillo Puerto Formation corresponds to the friable calcarenites exposed over the island (Figure 2). At least three different depositional environments are recognized in this unit, finishing with caliche 2 (Figures 7, 9a).

#### Multiphase-Flank Margin Caves

The multiphase-FMCs (Chempita, Chenchón, and Chechen Ha) are in the flanks of the ancient central cay. The vadose zone is developed through a massive sandstone without sedimentary structures due to the high weathering, growing through both lithostratigraphic units reaching the water table (Figure 9a).

In the vadose zone, thin sections show a wackestone-packstone with peloids and coated bioclasts. The bioclasts comprise green algae (*Halimeda*), mollusks (bivalves and gastropods), and benthic foraminifera such as Miliolids, Rotalids, and Soritids with small numbers of red algae (Figure 9b–9c). A micritic matrix with some

drusy cement is also seen (Figure 9b–9c). These facies are consistent with SMF 16, deposited at FZ-8, and associated with a decrease in energy level, representing the protected interior platform.

The texture below caliche 1 and caliche 0 is a coral framestone of highly micritized bioclast and peloids. Abundant pellets, peloids, echinoderms, benthic foraminifera, and reef-derived organisms like bryozoa and red algae also appear (Figure 9d–9e). Blocky or drusy cement is frequent, and the diagenesis strongly affects the corals, with the conversion of aragonite to blocky calcite. These characteristics correspond to SMF 5 and SMF 7, deposited at FZ-5, platform margin reef.

#### Classic Flank Margin Caves

Classic FMCs also appear at the flanks of the ancient central cay (Nohoch Hool, Ariadna, and Mariposa) but only in the calcarenites between caliche 1 and caliche 2. Host rock is a wackestone-packstone of peloids and coated bioclasts. The bioclasts contain green algae (*Halimeda*), mollusks (bivalves and gastropods), and benthic foraminifera such as Miliolids, Rotalids, and Soritids with small numbers of red algae (Figure 9b–9c). The matrix is micritic. However, the drusy cement also occurs (Figure 9b). These characteristics allow its classification as SMF 16, deposited at FZ-8, associated with a decrease in energy level on the protected interior platform.

#### Banana hole Flank Margin Caves

Banana hole FMCs are in the ancient beach ridges growing exclusively in the unit of carbonate sandstones. They display unlaminate (Figures 10a, 10c) parallel to low-angle cross-stratification in Cedral, Buenavista, and San Gervasio areas (Figures 4d–4f). A particular case is the herringbone stratification in the Murciélagos BH and Magnolia caves (Figure 4d). In Cantera Transversal and Chaac Mol caves, ichnofossil burrows such as *Glossifungites* sp. are present

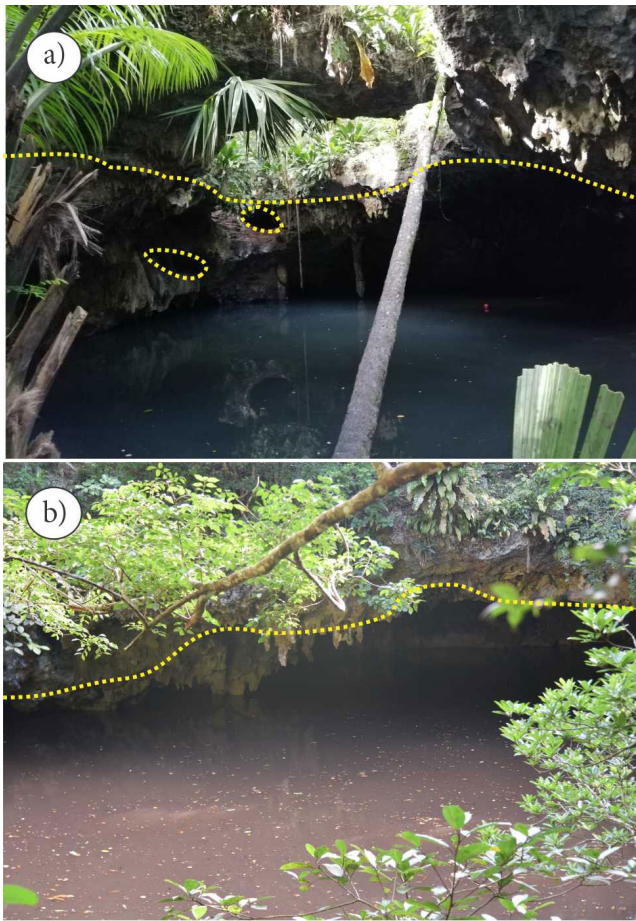


Figure 5. Multiphase flank margin caves. (a) Chempita cenote. (b) Chenchón cenote. The subaerial portion with globular chambers is shaped above the water table. Dashed lines define the upper limit of the main chamber, and dashed small circles indicate adjacent small globular chambers.

(Figure 10b). Additionally, shell concentrations or coquinas appear in the lower part of the unit in Cantera Transversal Cave. Scattered rhizoconcretions (Cedral area and Cantera Transversal) and black pebbles (Cantera Transversal cave) are also observed in the host rocks (Salgado-Garrido *et al.*, 2022).

The northern part of the island displays a well-sorted and rounded grainstone of bioclast and peloids with scattering ooids and lumps (Figure 10d). Within the bioclast, some mollusks (bivalves and gastropods), green algae (*Halimeda*), foraminifera (millioids), and coral fragments appear. Consistent with the SMF 11 and SMF 15 deposited in the FZ-6 (subtidal and supratidal sand-shoals). Furthermore, two generations of cement, circumgranular (primary) and granular (secondary), are identified (Figure 10e), illustrative from the meteoric-phreatic or vadose-phreatic zone.

In caves of the Cedral area, the microfacies are grainstone of the peloids and aggregated grains. There is an increase of lumps, ooids, intraclast, and peloids and a decrease in the coated bioclasts abraded skeletal grains compared to the north and east parts of the island (Figure 10f–10g). As in the previous microfacies, circumgranular and drusy-granular types of cement are detected (Figure 10g). Five standard microfacies SMF10, 11, 12, 15, and 17, constituted the host rock of the caves, all deposited in the open marine platform interior (FZ-7).

All studied host rock shows an upward shoaling from subtidal to supratidal facies, ending with the development of caliche 2, classic

evidence of meteoric affectation processes with pedogenetic carbonate development or FZ-10.

### Surface terrace map and paleo island emerged areas

The morphostratigraphic features and data of the terrace map of Cozumel from Salgado-Garrido *et al.* (2022) represent ancient emerging areas of the island. We obtained two hypothetical ancient, emerged areas related to FMC development during the last highstand sea level MIS 5e at +6 m a.s.l. (Blanchon *et al.*, 2009) and the current terrace map with FMC distribution.

The first emerged area corresponds to atoll-like morphology or terrace III, composed of an ancient central cay with a perimeter of 27.2 km and an area of 22.8 km<sup>2</sup> and ancient narrow strip islands that have a perimeter of 62.6 km and an area of 21.1 km<sup>2</sup> (Table 3). The second geometry (Figure 11b) represents an emerged area in which the lagoon is exposed into the vadose zone (terraces II and III), increasing the island size with a perimeter of 113.2 km and an area of 201.6 km<sup>2</sup> (Table 3). Finally, the current Cozumel Island emerged area is 470 km<sup>2</sup> while the perimeter corresponds to 116.25 km (Figure 11c; Table 3).

## DISCUSSION

In eogenetic limestone with stable tectonic conditions, like the Mexican Caribbean region and especially on the island of Cozumel, the morphostratigraphy features such as sedimentary units, karstic landforms, terraces, and FMCs are driven by sea-level variations.

Notably, the distribution and altimetric position of Cozumel FMCs in terrace II and III are proxies for maximum sea-level position and paleo coastline during the last highstand sea-level MIS 5e following coral records in the YP (Blanchon *et al.*, 2009) and similar behavior to The Bahamas archipelago FMCs (Mylroie & Carew, 1990; 1995a, 1995b; Kerans *et al.*, 2019; van Hengstum *et al.*, 2011; 2015).

### Flank margin cave speleogenesis on the Cozumel Island

Based on the Cozumel FMC morphology, distribution, and microfacies analysis, we classified them into three types of caves as follows: classical, multiphase, and banana holes subtype of FMCs (Mylroie *et al.*, 2016; Mylroie & Mylroie, 2017a). The classical FMCs correspond to the isolated caves Nohoch Hool, Ariadna, and Mariposa. In contrast, the multiphase FMCs correspond to cenotes Chempita, Chenchón, and Chechen Ha, where the subaerial portion displays flank margin cave morphology, and the subaquatic part shows multiple overprinting events enhancing its vertical extension. Both the classical and multiphase FMCs developed at the flanks of the ancient central cay or terrace III (Figure 3).

On the other hand, the banana holes FMC morphology pertains to caves developed on the ancient beach ridge progradation at the flank of terrace III corresponding to an ancient narrow strip island and flat terrains on terrace II represented by caves in San Gervasio, Buenavista, and Cedral areas, as well as Murcielagos BH, and Cantera Transversal caves (Figure 3).

### Classical and multiphase flank margin caves

Microfacial analysis shows that classical and multiphase FMCs in Cozumel evolved similarly to their coetaneous caves in Australia and The Bahamas (Eberhard, 2004; Grimes, 2006; Mylroie, 2013). During the early last highstand MIS 5e, the establishment of sand shoals or narrow strip islands favored the protected lagoon conditions that resemble the atoll-like morphology. At the same time, the ancient central cay developed over protected lagoon facies (Salgado-Garrido *et al.*, 2022). Both ancient central cay and narrow strip

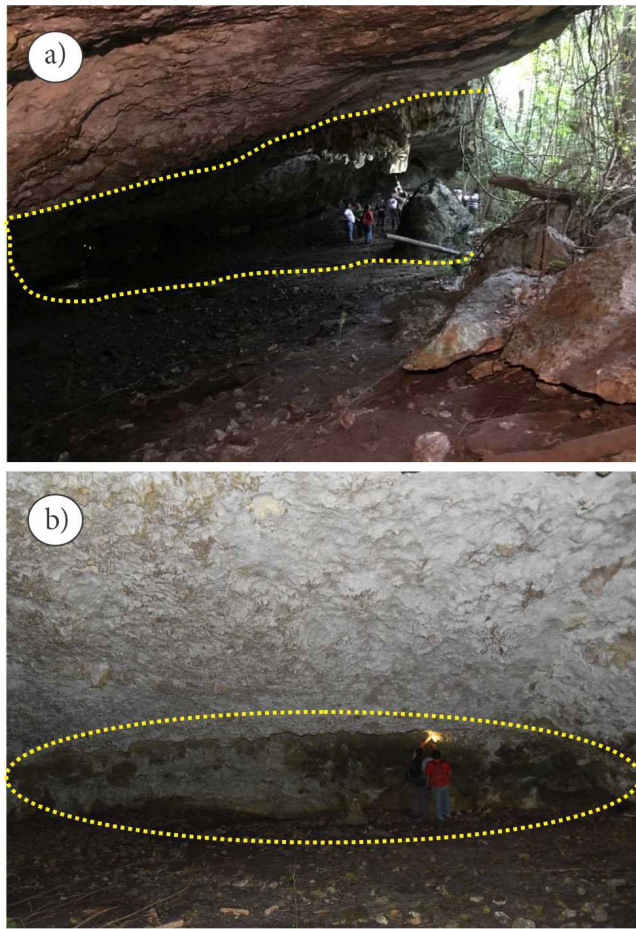


Figure 6. Classic flank margin caves. Nohoch Hool cave (a) chamber cross-section is shown by the dashed line, (b) phreatic chamber marked by the dashed line.

islands must have reached their maximum height during the late last highstand sea-level MIS 5e, represented by terrace III at 16 m a.s.l. (Figure 11a).

By stabilizing the ancient central cay, the area of ~22.8 km<sup>2</sup> triggers the formation of a freshwater lens and the stratification of the underground water (Figure 12a). According to Larson and Mylroie (2018), this area is enough to establish a freshwater lens with diffuse flow, but it is too small to allow turbulent flow.

The conditions for the FMC development started with the establishment of the mixing zone (Figure 12a). The phreatic morphologies observed at 6 m a.s.l. are concordant with diffuse subterranean flow through the matrix or interparticle porosity of eogenetic diagenesis (Vacher & Mylroie, 2002). Pore size increases by the connecting pores, reaching dimensions such as FMCs (Breithaupt *et al.*, 2021a).

During the MIS 5e in the Mexican Caribbean region, coral data support the hypothesis that sea level reached +6 m a.s.l. (Blanchon *et al.*, 2009). Which coincides with the apparition of the phreatic chambers of the classic and multiphase FMCs in the terrace II and flanks of terrace III.

#### **Flank margin caves in ancient beach ridges progradations**

The banana holes were previously reported in The Bahamas archipelago, and their origin remains controversial. Some authors claim a polygenetic genesis such as epikarstic vadose influence (Gulley

*et al.*, 2015; 2016; Whitaker & Smart, 1989), phreatic origin (Harris *et al.*, 1995), related to early syngeneses (Grimes 2006; Mylroie *et al.*, 2016; Mylroie & Mylroie, 2017a), and lastly, it is considered that banana holes can develop and increase in size from a transient water table perched aquifer, overprinting the initial porosity (Breithaupt *et al.*, 2021b).

However, Cozumel banana holes exhibit a more complex cave morphology and have a larger area footprint than banana holes in The Bahamas (Table 2).

The host rock of Cozumel banana holes is composed of grainstone bioclasts, with peloids associated with circumgranular and drusy cement (Figure 10), along with herringbone stratification (Murciélagos BH, and Magnolia caves), burrow structures (Cantera Transversal, and Chac Mool caves), and parallel-to-low cross-stratification (Figure 4d, 4e). The microfacies of the host rock in the Cantera Transversal, Murciélagos BH, Buenavista, and San Gervasio caves have an increase in bioclast with scattered ooids and intraclasts (Figures 10d–10e), consistent with classical sands shoals or FZ-6 (Flügel, 2010), while the Cedral caves (Aktum Balam, Track, Escondida and Ferchango caves), show an increase in ooids, lumps, and intraclasts (Figure 10f–10g) corresponding to platform interior open marine facies, or FZ-7. These facies match with subtidal inner platform open marine conditions with large primary porosity deposited in subtidal conditions during the last highstand sea level, which currently represents terraces II and III (Figure 3).

Ooid and lump-rich facies are reported during the MIS 5e in Caribbean islands such as The Bahamas, Cayman Islands, and Florida Keys (Harris, 2019; Jones & Hunter, 1990; Kerans *et al.*, 2019; Kindler & Hearty, 1996; Mylroie *et al.*, 2016; Purkis & Harris, 2016). Oolitic-peloidal facies indicate major flooding events in the Bahamas Bank during the last highstand MIS 5e (Kindler & Hearty, 1996). Both depositional textures FZ-6 and FZ-7 in Cozumel banana holes represent two different depositional environments very close to each other, and similar facies have been reported in cave walls over Bahamas island (Mylroie *et al.*, 2016; Schwabe *et al.*, 1993).

During the late last highstand sea-level MIS 5e the ancient narrow-strip islands (terrace III) had a hypothetical area of 21 km<sup>2</sup> (Figure 11a, Table 3), allowing the establishment of an asymmetric freshwater lens (Vacher, 1988) with the diffuse subterranean flow (Larson & Mylroie, 2018) allowing the development of flank margin-type phreatic morphologies (Figure 12b). At this time, the ancient beach ridge prograded to the leeward of narrow strip islands (Salgado-Garrido *et al.*, 2022), assisted by sediment transport from E-W trade winds (Gischler & Lomando, 1999, 2000) via the ancient tidal channels (Figures 3b, 3c).

The spatial correlation between the location of ancient beach ridge progradations and the distribution of banana holes on Cozumel suggests that paleo-coast migration occurred in tandem from the island core outwards (Figures 11b–11c, 12b) according to the banana hole model (Mylroie *et al.*, 2016; Mylroie & Mylroie 2017a). The ancient beach ridge progradation and Cozumel banana holes developed as sediment mobilization filled the protected lagoon, probably during stillstand conditions of the last highstand sea-level MIS 5e forming the terrace II (Salgado-Garrido *et al.*, 2022), joining the sand islands (ancient central cay and narrow strips) into a single larger island (Figures 11b, 12c); in the same way as the morphostratigraphic model in The Bahamas archipelago of Kindler and Hearty (1996).

We delineated the hypothetical emerged area of Cozumel, including the sand islands and protected lagoon areas (terraces II and III), a total emerged area of 201.6 km<sup>2</sup> (Figure 11b and Table 3). With these dimensions, Cozumel Island maintains a diffuse-laminar flow drainage system, likely evidenced by the significant number of closed depressions identified in the Cedral area at the terrace II from

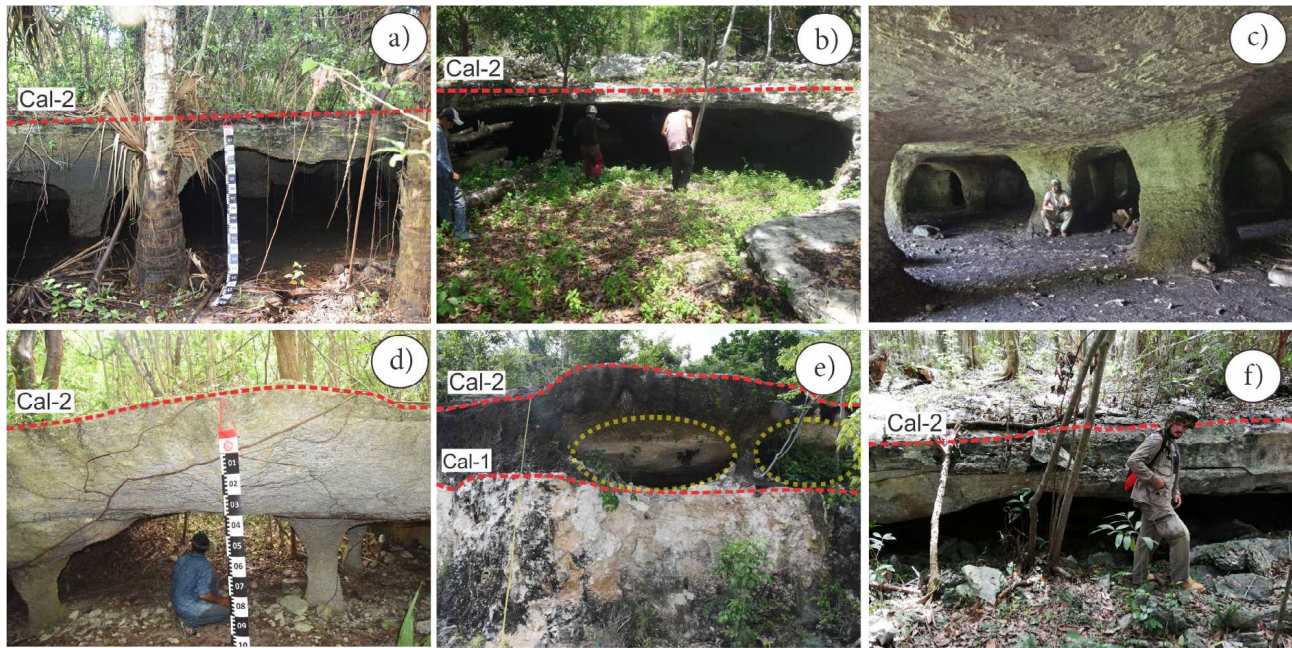


Figure 7. Banana hole flank margin caves. Cave morphologies and diverse residual pillars. (a) Escondida cave, Cedral area, with vast residual pillars. (b–c) Buena Vista cave entrance and vast residual pillars and flat ceilings. (d) Ferchango cave, Cedral area. (e) Cantera Transversal cave, in the north part of the island, has a dashed yellow line that represents phreatic morphology with an intermediate pillar. (f) Murciélagos BH Cave is in the north part of the island. Red dashed lines point to Caliches 1 (Cal-1) and 2 (Cal-2). Cal-1 is below the FMC.

satellite imagery (Rodríguez-Castillo *et al.*, 2021) which can reach phreatic chambers. The increased area in the terrace II, and diffuse and laminar subterranean flow continued to operate efficiently during lagoon infilling until it reached the size threshold for developing turbulent flow drainage in an island with at least 10 km of radius and emerged area of 314 km<sup>2</sup> (Larson & Mylroie, 2018). Therefore, isolated

chambers or phreatic morphologies with little horizontal development within the predicted island size and altitude between 3–6 m a.s.l. are potentially FMCs or part of them.

The Cozumel FMCs appear above the current relative sea-level position in a scattered and isolated distribution (Figures 11c, 12d). From a karst hydrogeology perspective, they represent the first

Table 2. Morphometric analysis of Cozumel FMCs. Cave areas are expressed in square meters (m<sup>2</sup>) while perimeters, entrance width (EW), and internal width (IW) are expressed in meters (m). A/P refer to area to perimeter ratio, EW/IW refer entrance width to internal width ratio, and AS/AL refer axis short to axis large. R. num = Register number of Supplementary table S1. Ch = chamber cave.

R. num	Cave name	Size	Perimeter (m)	Area (m <sup>2</sup> )	Ch height (m)	EW (m)	IW (m)	AS (m)	AL (m)	A/P	EWIW	AS/AL
20	Cantera Trans	Small	21.37	26.54	1	7.17	7.17	7.25	6.5	1.24	1	1.11
25	Chichan Nah	Small	25.81	33.46	1.7	1.52	10.22	5.38	10.3	1.29	0.14	0.52
19	Murcielagos BH	Small	40.84	42.71	0.8	15.59	15.59	7.2	16.02	1.04	1	0.44
21	Piramide	Small	38.85	97.42	2	6.07	12.03	12.07	12.44	2.5	0.5	0.97
24	El Lina	Medium	45.68	121.98	1	13.39	16.85	9.67	16.08	2.67	0.79	0.6
22	Chaac Mool	Medium	50.78	170.91	3.7	4.97	15.95	15.22	16.32	3.36	0.31	0.93
3	Palma Secuestrada	Medium	79.06	256.71	1.8	20.95	26.6	17.89	26.67	3.24	0.78	0.67
4	Palmar	Medium	140.7	384.66	1.3	24.2	37.95	33.08	39.49	2.73	0.63	0.83
23	Kana Nah	Medium	95.52	401	2	8.89	31.95	25.56	26.58	4.19	0.27	0.96
40	Cenote Chempita	Medium	106.9	428.46	6	16.2	39.74	23.97	37.44	4	0.4	0.64
5	Ferchango	Medium	144.68	444.37	1.65	12.89	34.3	24.27	34.72	3.07	0.37	0.69
18	Nohoch Hool	Medium	108.95	465.66	5	41.98	41.98	23.14	42.22	4.27	1	0.54
16	Magnolia	Medium	120.49	568.44	2.1	19.99	34.4	26.62	34.05	4.71	0.58	0.78
41	Cenote Chenchon	Medium	111.54	799.72	6	28.13	33.72	30.26	36.21	7.16	0.83	0.83
26	Est. San Gervasio	Medium	156.93	857.53	2.7	27.7	48.55	39.93	48.1	5.46	0.57	0.83
17	Buenavista	Large	230.78	1045.79	1.8	24.53	53.6	41.74	54.24	4.53	0.45	0.76
6	Aktun Balam	Large	175.54	1171.91	1.8	23.79	28.79	35.68	54.46	6.67	0.82	0.65
7	Cedral track	Large	291.83	2340.28	1.7	110	115	34.6	115	8.01	0.95	0.3
	mean values		110.35	536.53	2.44	22.66	33.57	22.97	34.82	3.9	0.63	0.72

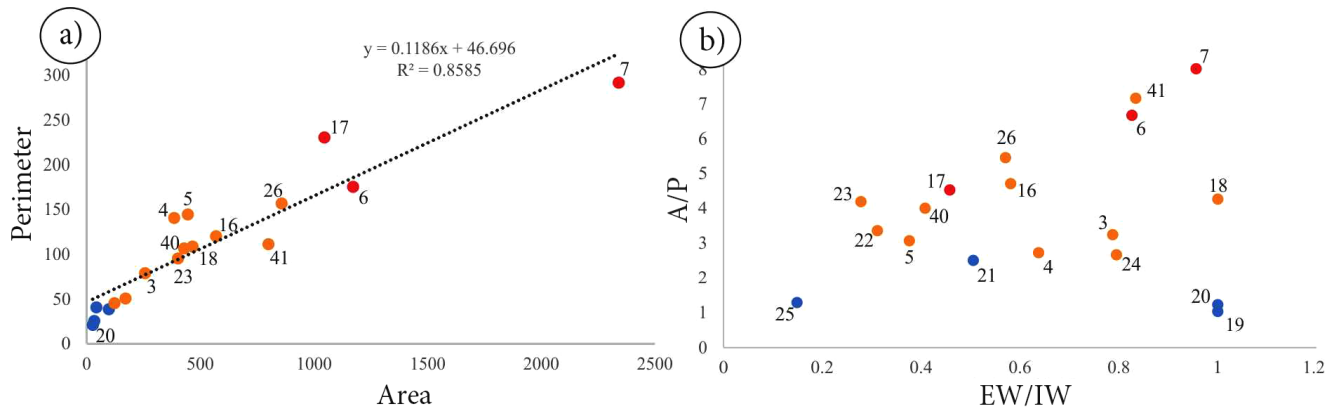


Figure 8. Plot of cave morphometry values of Cozumel flank margin caves. a) Plot perimeter vs area  $R^2 = 0.85$ . b) Plot Area to perimeter ratio (A/P) vs EW/IW. Color circles represent the cave size: blue= small, orange= medium, red= large. Data from Table 2.

hydrogeological groundwater systems established in the calcarenites with laminar and diffuse flows (Larson & Mylroie, 2018) and an asymmetric freshwater lens in the sand islands (Vacher, 1988).

**The role of karst denudation factor**

The modern maximum island height was probably higher, as the model of Salgado-Garrido *et al.* (2022) did not consider the karst denudation factor, which for eogenetic limestones has been calculated as 42 mm  $ky^{-1}$  (Mylroie & Mylroie, 2017b). However, the model considers a homogeneous karstification over the whole island, preserving the altimetric differences in the depositional environment in the different terraces.

Classical and multiphase FMCs in Cozumel have medium to large entrances, with phreatic chambers reaching up to ~6 m in height and up to 9 m of the vadose zone. On the other hand, Cozumel banana holes exhibit small, medium, and large sizes with a height restricted to 2.5 m with a vadose zone. The morphometric values EW/IW, and

AS/AL ratios (Table 2) reaffirm the Cozumel FMCs origin as opposed to sea caves, despite high values in ratios, which are unexpected for FMCs (Waterstrat *et al.*, 2010). However, high values in the EW/IW and AS/AL ratios point to different grades of overprinting or erosion processes (Table 2).

The denudation karst factor for eogenetic environments in the Guam archipelago suggests a reduction of ~5 m in rock thickness in the last 120 ky (Mylroie & Mylroie, 2017b). Consequently, the Cozumel Island would presumably have reached up to 21 m a.s.l. in the central cay and terrace III and up to 11 m in terrace II and flat terrain. This value could partially explain the presence of FMC (Multiphase-FMC) with a larger vadose zone and fewer caves discovered in the center of the island. There would be a larger volume of rock to dissolve before intercepting with an FMC.

However, considering the karst denudation factor calculated in the Guam archipelago, the ancient beach ridge progradations and tidal channels could have disappeared, removing geomorphic evidence

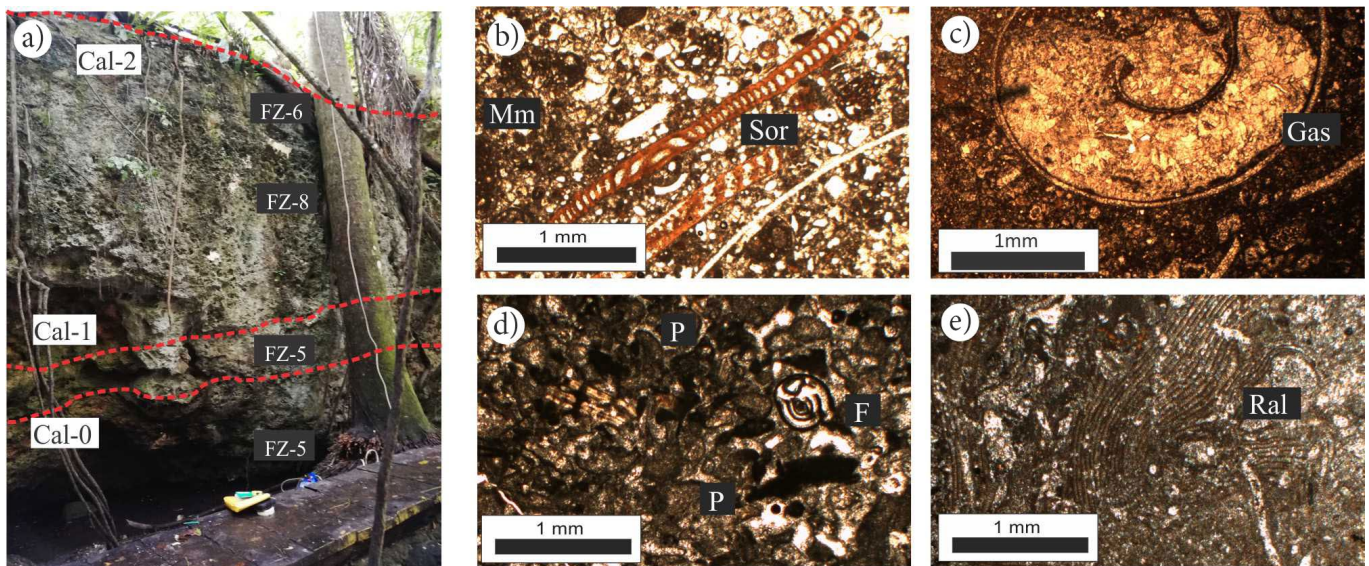


Figure 9. Host rock and microfacies analysis multiphase and classic flank margin caves. (a) Stratigraphic section inside cenote Chempita, red dashed lines point to the caliches (Cal) or stratigraphic boundaries. The facies zone (FZ), according to microfacies analysis. (b–c) Corresponds to FZ-8 wackestone packstone with foraminifera Sorites sp. (Sor), Gastropods (Gas) and micritic matrix (Mm); b) Nohoch Hool sample. c) Chempita cenote sample. d–e) Chempita cenote samples below caliche 1, composed of wackestone-packstone with bioclasts e.g., foraminifera (F), reef-derived organisms like bryozoa and red algae (Ral), abundant pellets (P). All photomicrographs with plane-polarized light.

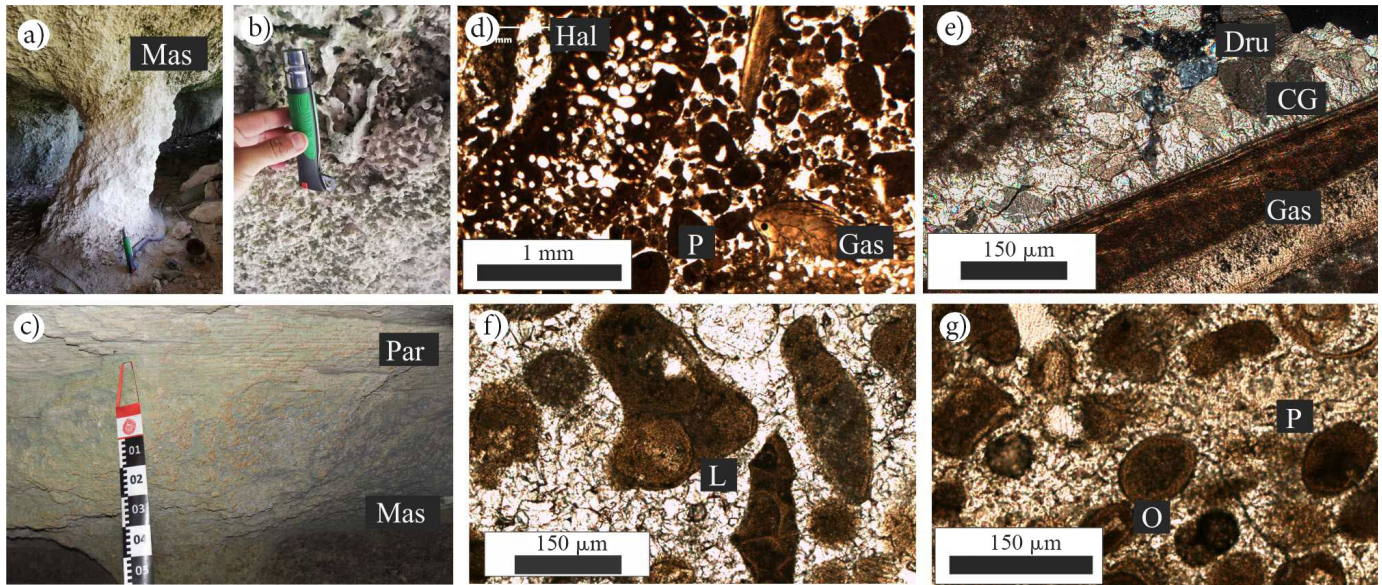


Figure 10. Host rock and microfacies analysis of banana hole flank margin cave. Cantera Transversal: a) residual pillar without stratification in a massive (Mas) calcarenite cave. b) Ichnofossil inside the cave, *Glossifungites* sp., scale is a 15 cm-knife. c) Massive calcarenites (Mas) below the parallel stratification (Par) in Aktun Balam Cave. d) Grainstone with bioclasts. Green algae: Halimeda (Hal), mollusk gastropod (Gas) and peloids (P). e) Grainstone of abundant bioclasts with two types of cement growing over gastropod (Gas): circumgranular (CG) and drusy (Dru). f) Grainstone of ooids, peloids, aggregate grain lumps (L) and bioclasts in Aktun Balam Cave. g) Grainstone ooids (O), peloids (P) in the transitional zone near the Cedral area. All photomicrographs were taken with plane-polarized light.

essential for banana hole recognition, such as beach ridge progradation environments and thin ceilings prone to collapse (Myroie & Myroie, 2017a). Therefore, due to the excellent feature preservation of Cozumel, this value should be lower than the calculated value in Guam. A possible explanation for a decrease in the computed value in Guam is the development of calcretes (Caliche-2), which are related to a warm or primarily dry climate (Valera-Fernández *et al.*, 2020) and a reduction in the initial porosity of the host rock during this pedogenetic process. Nonetheless, more detailed research is essential

on the role of calcrete formation and its relationship to hydrogeological processes on Cozumel Island and karstic areas.

#### The areal footprint of Cozumel flank margin caves and the overprinting process

Cozumel FMCs have preeminent values of EW/IW including small and large banana holes, classical and multiphase FMCs with an average EW/IW ratio of 0.637 (Table 2), which is greater than the Bahamas with 0.524, close to 0.672 in Puerto Rico (Lace, 2008; Waterstrat *et*

Table 3. Cozumel Island emerged areas. Refers to areas above sea level. First hypothetical island corresponds to island of Cozumel when the sea level reaches the peak during last highstand sea level MIS 5e in atoll-like morphology with ancient central cay (Salgado-Garrido *et al.*, 2022) at 6 m asl from current sea level position (Blanchon *et al.*, 2009). Second hypothetical island corresponds to island shape if the atoll-like morphology (hypothetical island 1) plus terrace II were exposed. NA refers to not applicable. MIS refer to marine isotopic stage when the karst morphologies were formed. \*The hypothetical circle island is the threshold size to form large epigenetic phreatic conduits from the model of Larson and Myroie (2018).

Cozumel Island Shape	Geomorphic features	Perimeter (km)	Area (km <sup>2</sup> )	Radius (km)	Size island	Subterranean flow	Conduit type	Cave morphology	MIS
Current shape	Terraces I, II, and II	116.24	469.93	~16	Large	Turbulent	Phreatic, vadose	Overprinting processes, multiphase	1
Largest than current	Terraces I, II, and II + larger emerged area	>	>	>	Large	Turbulent	Phreatic, vadose, and maximum deep	Overprinting processes, multiphase	5d to 2
Second hypothetical island II	Terrace II and III	113.26	201.60	<	Small	Difusse	Isolated FMC	Flank margin and chamber fusions	5e late
First hypothetical island (Atoll-like)	Ancient central cay (Terrace III)	27.26	22.83	<	Small	Diffuse	Isolated FMC	Flank margin and chamber fusions	5e early
	Ancient narrow strip islands (Terrace III)	62.60	21.13	<	Small	Diffuse	Isolated FMC	Flank margin and chamber fusions	
Hypothetical circle island*	NA	62.83	314.17	10	Large	Turbulent	Phreatic conduit	NA	NA

*al.*, 2010) but less than Tinian Island with ca. 1 (Waterstrat *et al.*, 2010). The values obtained in the Bahamas, Puerto Rico, and Tinian Islands, were collected before classifying banana holes as a subtype of flank margin caves so that they could have a bias of speleogenetic origin between the types of FMCs, but the EW/IW ratio can provide relevant information about the modification processes of this type of cavities (Lace, 2008; Waterstrat *et al.*, 2010). The EW/IW and karst denudation factor values in Tinian Islands point to a higher denudation than Cozumel Island (Myroie & Myroie, 2017b; Stafford *et al.*, 2005).

On the other hand, the EW/IW ratios in Puerto Rico and Cozumel Island are close values, representing the high modification degree (Lace, 2008) attached to mechanical and diagenetic overprinting processes (Breithaupt *et al.*, 2021b; Grimes, 2006; Lace, 2008), finally, limited Cozumel FMC data may increase the values proposed in Bahamas FMCs. The Cozumel FMC distribution and morphometric ratios are consistent with ancient shoreline positions, as suggested by high values in the AS/AL ratios, reflecting the lateral extension or elongation of the cave morphologies parallel to ancient shorelines (Waterstrat *et al.*, 2010). In contrast, the sizes and footprint cave values are ambiguous, especially in Cozumel banana holes, due to small and simple caves (Cedral and Buenavista caves) exhibited in the same landscape as medium and large size caves with more complex morphologies. These larger caves have increased pendant structures and pillars reflecting chamber fusion, *e.g.*, Ferchango, Track, Aktum Balan, Buenavista, and Magnolia caves. The uncommon case corresponds to the Cedral Track cave, which has the largest footprint area and EW/IW ratio, with fewer pillars.

In Puerto Rico and The Bahamas (Lace, 2008; Waterstrat *et al.*, 2010), the A/P and EW/IW vs A/P allow the separation of caves by origin, but our data does not support this separation among the analyzed caves reaffirming the common origin of all FMCs despite some morphological differences (Figure 7). In this way, the size of FMCs in Cozumel can be the result of the action of aggressive solutions created in adjacent swampy environments, as reported in Australia (Grimes, 2006) or by the influx and oxidation of organic matter, as in The Bahamas (Bottrell *et al.*, 1993; Gulley *et al.*, 2013, 2015, 2016; Myroie & Myroie, 2017a; Stoessell *et al.*, 1993). This possibility is

supported by the black pebbles in the host rock in Cantera Transversal (Salgado-Garrido *et al.*, 2022).

Another scenario to explain the size of FMCs in Cozumel is the implantation of a water table perched aquifer (Breithaupt *et al.*, 2021b). This model does not require the expected period during the MIS 5e event to dissolve large volumes of carbonates and can even use a pre-existing small FMC or develop a new similar structure. Still, the water table perched aquifer model does not explain the difference between cave sizes in the same geographical region.

The classical FMC model in The Bahamas contemplates that the FMC size is connected to the stability of the sea-level position or mixing zone residence time, especially during the MIS 5e (Labourdette *et al.*, 2007; Larson & Myroie, 2018; Myroie *et al.*, 1990, 1995a, 1995b; Roth *et al.*, 2006; Waterstrat *et al.*, 2010). Nevertheless, the interval, sub-phases, and maximum range of MIS 5e are still under discussion. Hearty *et al.* (2007) consider that the average duration of MIS 5e worldwide is  $130 \pm 2$  to  $119 \pm 2$  ky without stable conditions. While in The Bahamas Thompson *et al.* (2011) suggest unstable conditions during  $123 \pm 1.2$  to  $114.4 \pm 1$  ky in opposition to stable conditions near to 10 ky (Chen *et al.*, 1991, Myroie & Myroie, 2007).

The sea level records during the last highstand MIS 5e in the Mexican Caribbean region differ from The Bahamas in substages and duration (Blanchon *et al.*, 2009; Moseley *et al.*, 2013). However, both records, plus Thompson *et al.* (2011) in The Bahamas, point to sea-level instability during the last highstand MIS 5e, advising that sea-level stability is not the only factor involved in Cozumel FMC size. Despite the differences between substages and FMCs size, Cozumel Island and The Bahamas share sedimentary units and cave patterns during the last highstand MIS 5e.

## CONCLUSIONS

The Cozumel flank margin cave distribution developed on terrace II and III at 6 m a.s.l., cave morphology, and morphometric analysis, as well host rock microfacies analysis, support that are proxies for ancient sea-level position and changes in the island landform during the last highstand MIS 5e consistent with the regional records.

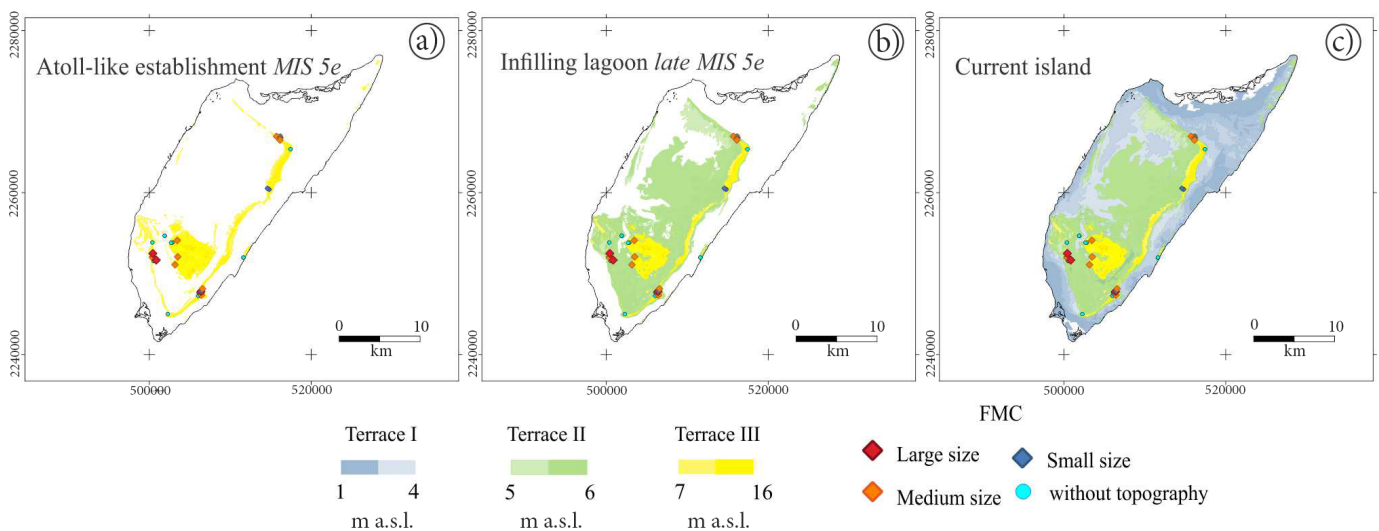


Figure 11. Cozumel island emerged areas. a) The first hypothetical emerged area corresponds to the ancient central cay and the narrow-strip island which had an atoll-like morphology, terrace III. b) The second hypothetical emerged area corresponds to the ancient central cay, narrow strip island, and lagoon, as well as terraces III and II. c) The current emerged area has three terraces. The diamonds and different colors represent FMC entrances. Database on Table 3.

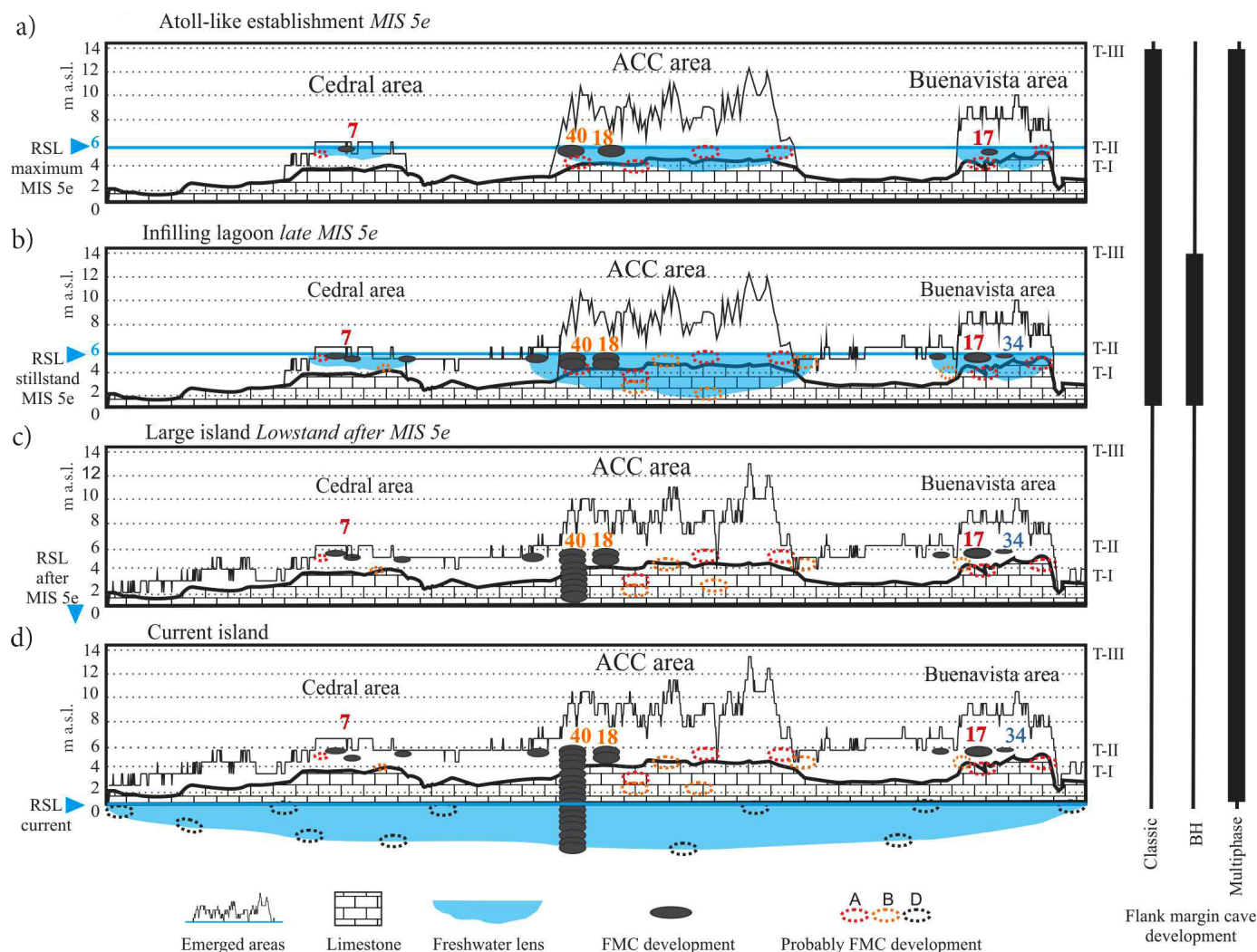


Figure 12. Speleogenetic flank margin cave model of Cozumel Island. Topographic profile X-X' from Figure 3 approximate W-E along the Cozumel Island. Based on the DEM data reconstruction model, the serrated line represents current (d) and hypothetical ancient profiles (a-b). On the right side, the width line represents the period of FMC development. a) Establish an atoll-like morphology with a central cay (terrace III) and freshwater lens on each island. Classical and multiphase FMCs form, reaching a maximum position at +6 m a.s.l. during the maximum last highstand sea-level MIS 5e. b) Island size increases during stillstand conditions, evidenced by ancient beach ridge and banana holes landforms, until it forms a single island (terraces II and III). c) Island size increases due to sea level fall, favoring the multiphase FMCs development d) Current Island of Cozumel with FMCs at the core of the island. RSL=relative sea-level. ACC= ancient central cay. BH= banana hole. Limestone represents Unit 1 or Fm. Carrillo Puerto.

The multiphase flank margin caves resulted from multiple overprinting processes from their formation until now and are closely related to some cenotes.

Cave patterns, geomorphic surface, and host rock microfacial analysis allows the identification of the banana holes, but their sizes and footprint cave values are ambiguous, hiding their origin.

Additional work is needed to clarify some morphometric data about flank margin caves compared to their coetaneous in other carbonate platforms.

### Acknowledgments

We acknowledge the support of Sara Griset, Orlando Gutiérrez, Daisy Valera, Bruno Chávez, Ofelia Beltrán, Lourdes Rodríguez, Angélica de la Cruz, Kay Vilchis, and Erick Sosa during fieldwork. We also want to thank Jaime Díaz-Ortega for contributing during the field sessions and obtaining the thin sections. Special thanks to

Emilio Novelo Flores and Mariano Dzay, the commissioners of the Villa Cozumel ejido, and to Fidel Ladrón de Guevara of Wild Tours Cozumel, Ramón Villanueva of Rancho Buenavista for providing access to the area. The manuscript was much improved after helpful comments by Dr. Daniel Ballesteros and an anonymous reviewer.

### Funding

Funding was provided by National Geographic Society grant W418-15, PAPIIT IN109323, and PAPIIT IN103617, and the Consejo Nacional de Ciencia y Tecnología (CONACyT) for the fellowship to support the Ph.D. studies of Hugo E. Salgado Garrido. The sponsorship of diving gear was provided by Santi Diving, Apeks, Ammonite Systems, and Casco Antiguo.

### Author Contributions

H.E.S.G., S.T.P., and R.L.M. conceived of the presented idea, writing, review, editing. E.S.R. writing, review and encouraged the

investigation about karst and calcretes. P.S., L.M.M.O., and G.Y. participated in cave explorations and manuscript review. All authors discussed the results and contributed to the final manuscript.

#### Data Availability Statement

All data are included in the text.

#### Declaration Of Competing Interests

The authors declare no competing interests.

#### SUPPLEMENTARY MATERIAL

Supplementary Table S1, can be found on the Abstract's preview page of this paper. <DOI: <http://dx.doi.org/10.22201/igc.20072902e.2024.3.1796>>

#### REFERENCES

- Athie, G., Candela, J., Sheinbaum, J., Badan, A., & Ochoa, J., (2011). Yucatan Current variability through the Cozumel and Yucatan channels. *Ciencias Marinas*, 37, 471–492.
- Bauer-Gottwein, P., Gondwe, B. R. N., Charvet, G., Marín, L., Rebolledo-Vieyra, M., & Merediz-Alonso, G., (2011). Review: The Yucatán Peninsula karst aquifer, Mexico. *Hydrogeology Journal*, 19, 507–524. <https://doi.org/10.1007/s10040-010-0699-5>
- Beddows, P., Blanchon, P., Escobar-Briones, E., & Torres-Talamante, O., (2007a) Los cenotes de la península de Yucatán. *Arqueología Mexicana*, 32–35.
- Beddows, P.A., Smart, P.L., Whitaker, F.F., & Smith, S.L., (2007b). Decoupled fresh–saline groundwater circulation of a coastal carbonate aquifer: Spatial patterns of temperature and specific electrical conductivity. *Journal of Hydrology*, 346, 18–32.
- Blanchon, P., Eisenhauer, A., Fietzke, J., & Liebetrau, V., (2009). Rapid sea-level rise and reef back-stepping at the close of the last interglacial highstand. *Nature*, 458, 881–884.
- Bottrell, S., Carew, J., & Mylroie, J.E., (1993). Inorganic and bacteriogenic origins for sulfate crust in flank margin caves, San Salvador Island, Bahamas. *Proceedings of the 6th Symposium on the Geology of The Bahamas, Bahamian Field Station, San Salvador, Bahamas*, 17–21.
- Breithaupt, C., Gulley, J.D., Moore, P.J., Fullmer, S.M., Kerans, C., & Mejia, J.Z., (2021a). Flank margin caves can connect to regionally extensive touching vug networks before burial: Implications for cave formation and fluid flow. *Earth Surface Processes and Landforms*, 46(8), 1458–1481. <https://doi.org/10.1002/esp.5114>
- Breithaupt, C.I., Gulley, J.D., Bunge, E.M., Moore, P.J., Kerans, C., Fernandez-Ibañez, F., & Fullmer, S.M., (2021b). A transient, perched aquifer model for banana hole formation: Evidence from Salvador Island, Bahamas. *Earth Surface Processes and Landforms*, 47(2), 618–638. <https://doi.org/10.1002/esp.5276>
- Butterlin, J., & Bonet, F., (1963). *Las Formaciones Cenozoicas de la parte mexicana de la Península de Yucatán: México*. Instituto de Geología, Universidad Nacional Autónoma de México.
- Cabadas-Báez, H., Solleiro-Rebolledo, E., Sedov, S., Pi-Puig, T., & Gama-Castro, J., (2010). Pedosediments of karstic sinkholes in the eolianites of N.E. Yucatán: A record of Late Quaternary soil development, geomorphic processes, and landscape stability. *Geomorphology*, 122, 323–337.
- Carew, J.L., & Mylroie, J.E., (1995). Depositional model and stratigraphy for the Quaternary geology of the Bahama Islands. In H. A. Curran, & B. White (Eds.), *Terrestrial and Shallow Marine Geology of the Bahamas and Bermuda* (300, 5–34). Geological Society of America Special Paper.
- Chen, J. H., Curran, H. A., White, B., & Wasserburg, G. J., (1991). The precise chronology of the last interglacial period: 234U-230Th data from fossil coral reefs in the Bahamas. *Geological Society of America Bulletin*, 103, 82–97.
- Choquette, P. W., & Pray, L. C., (1970). Geologic nomenclature and classification of porosity in sedimentary carbonates. *American Association of Petroleum Geologist Bulletin*, 54, 207–250.
- Dillon, W. P., & Vedder, J. G., (1973). Structure and development of the continental margin of British Honduras: *Geological Society of America Bulletin*, 84, 2713–2732.
- Dunham, R., (1962). Classification of carbonate rocks according to depositional texture. In W. Ham (Ed.), *Classification of Carbonate Rocks* (1, 108–121). American Association of Petroleum Geologists, Memoir.
- Eberhard, S. M. (2004). Ecology and Hydrology of a Threatened Groundwater-Dependent Ecosystem: The Jewel cave karst system in Western Australia, [Ph.D. Thesis] University of Murdoch, Australia.
- Embry, A., & Klovan, J. (1971). A late Devonian reef tract on Northeastern Banks Island Northwest Territories. *Bulletin of Canadian Petroleum Geologist*, 730–781.
- Emery, K. O., & Uchupi, E., (1972). Western North Atlantic Ocean: Topography, rocks, structure, water, life, sediment. *American Association of Petroleum Geologist Memoir*, 17.
- Flügel, E., (2010). Microfacies of carbonate rocks analysis, Interpretation and application. Springer-Verlag Berlin Heidelberg, 984 pp.
- Frausto-Martínez, O., Angelica Zapi-Salazar, N., & Colin-Olivares, O. (2019). Identification of Karst Forms Using LiDAR Technology: Cozumel Island, Mexico. *IntechOpen*. doi: 10.5772/intechopen.79196
- Frontana-Urbe, S., & Solís-Weiss, V. (2011). First Records of Polychaetous Annelids from Cenote Aerolito (Sinkhole and Anchialine Cave) in Cozumel Island. *Journal of Cave and Karst Studies*, 73(1), 1–10.
- Gischler, E., & Lomando, A. J., (1999). Recent Sedimentary facies of isolated carbonate platforms, Belize-Yucatan system, Central America. *Journal of Sedimentary Research*, 69, 747–763.
- Gischler, E., Lomando, A. J., (2000). Isolated carbonate platform of Belize, Central America: sedimentary facies, late Quaternary history and controlling factors. *Geological Society, London, Special Publications*, 178, 135–146.
- Grimes, K. G., (2006). Syngenetic Karst in Australia: a review. *Helveticite*, 39, 27–38.
- Gulley, J. D., Martin, J. B., Moore, P. J., & Murphy, J., (2013). Formation of phreatic caves in an eogenetic karst aquifer by CO<sub>2</sub> enrichment at lower water tables and subsequent flooding by sea level rise. *Earth Surface Processes and Landforms*, 38, 1210–1224.
- Gulley, J. D., Martin, J. B., Moore, P. J., Brown, A., Spellman, P. D., & Ezell, J., (2015). The heterogeneous distribution of CO<sub>2</sub> may be more important for dissolution and karstification in coastal eogenetic limestone than mixing dissolution. *Earth Surface Processes and Landforms*, 40, 1057–1071.
- Gulley, J. D., Martin, J. B., & Brown, A., (2016). Organic carbon inputs, common ions and degassing: rethinking mixing dissolution in coastal eogenetic carbonate aquifers. *Earth Surface Processes and Landforms*, 41, 2098–2110.
- Harris, P.M., (2019). Lessons from a modern carbonate sandbody- A personal experience of comparative sedimentology. *The Depositional Record*, 5, 438–450.
- Harris, J. G., Mylroie, J. E., Carew, J. L., (1995). Banana holes: Unique karst features of the Bahamas. *Carbonates and Evaporites*, 10, 215–224.
- Häuselmann, Ph. (2011). UIS Mapping Grades. *International Journal of Speleology*, 40, IV–VI.
- Hearty, P. J., Hollin, J. T., Neumann, A. C., O'Leary, M. J., McCulloch, M. (2007). Global sea-level fluctuations during the Last Interglaciation (MIS 5e). *Quaternary Science Reviews*, 26, 2090–2112.
- Heeb, B., 2013. DistoX2 Calibration Manual. Paperless Cave Surveying 1-3, Available at <https://paperless.bheeb.ch/>. (Accessed 10 November 2023).
- Instituto Nacional de Estadística y Geografía (INEGI), 2020a, Red Geodésica Nacional Activa. Instituto Nacional de Estadística y Geografía. [https://www.inegi.org.mx/temas/geodesia\\_activa/](https://www.inegi.org.mx/temas/geodesia_activa/). (accessed 2 February 2021).
- Instituto Nacional de Estadística y Geografía (INEGI), 2020b, Modelo digital de elevación de alta resolución Lidar 2008. Modelo digital de elevación de alta resolución Lidar 2008, Tipo TERRENO T. Instituto Nacional de Estadística y Geografía. <https://www.inegi.org.mx/app/biblioteca/ficha.html?upc=702825998578> (accessed 2 February 2021).
- Jones, B., & Hunter, I. G. (1990). Pleistocene paleogeography and sea levels on the Cayman Islands, British West Indies. *Coral Reefs*, 9, 81–91. <https://doi.org/10.1007/BF00368803>
- Kelley, K. N., Mylroie, J. E., Mylroie, J. R., Moore, C., Collins, L., Ersek, L., Lascu, I., Roth, M., Moore, P., Passion, R., & Shaw, C. (2006). Eolianites

- and karst development in the Mayan Riviera in Mexico., in *Proceedings of the 12th Symposium on the Geology of the Bahamas and Other Carbonate Regions*, 88–99.
- Kerans, C., Zahm, C., Bachtel, S. L., Hearty, P., & Cheng, H. (2019). Anatomy of a late Quaternary carbonate island: Constraints on timing and magnitude of sea-level fluctuations, West Caicos, Turks and Caicos Islands, BWI. *Quaternary Science Reviews*, 205, 193–223.
- Kindler, P., & Hearty, P. J. (1996). Carbonate petrography as an indicator of climate and sea-level changes: new data from Bahamian Quaternary units. *Sedimentology*, 43, 381–399.
- Labourdette, R., Lascu, I., Mylroie, J. & Roth, M. (2007). Process-like modeling of Flank-Margin caves: From Genesis to burial evolution. *Journal of Sedimentary Research*, 77, 965–979.
- Lace, M. J. (2008). Coastal cave development in Puerto Rico. *Journal of Coastal Research*, 24, 508–518.
- Larson, E., & Mylroie, J., (2018). Diffuse Versus Conduit Flow in Coastal Karst Aquifers: The Consequences of Island Area and Perimeter Relationships. *Geosciences*, 8, 268. <https://doi.org/10.3390/geosciences8070268>
- López-Ramos, E., (1973). Estudio Geológico de la Península de Yucatán. *Boletín Asociación Mexicana de Geólogos Petroleros*, 25, 23–76.
- Lugo-Hubp, J., Aceves-Quesada, J., & Espinasa-Pereña, R. (1992). Rasgos geomorfológicos mayores de la Península de Yucatán. *Universidad Nacional Autónoma de México, Instituto de Geología, Revista*, 10, 143–150.
- Mejía-Ortiz, L. M., Yáñez, G., López-Mejía, M., & Zarza-González, E., (2007). Cenotes (anchialine caves) on Cozumel island, Quintana Roo, México. *Journal of Cave and Karst Studies*, 69, 250–255.
- Moseley, G. E., Smart, P. L., Richards, D. A., & Hoffmann, D. L., (2013). Speleothem constraints on marine isotope stage (MIS) 5 relative sea levels, Yucatan Peninsula, Mexico. *Journal of Quaternary Science*, 28, 293–300.
- Moseley, G. E., Richards, D. A., Smart, P. L., Standish, C. D., Hoffmann, D. L., ten Hove, H., & Vinn, O., (2015). Early–middle Holocene relative sea-level oscillation events recorded in a submerged speleothem from the Yucatán Peninsula, Mexico. *The Holocene*, 25, 1511–1521.
- Mylroie, J.E., (2013). Coastal karst development in carbonate rocks. In M. Lace, & J. Mylroie (Eds.) *Coastal karst landforms*. (5, 77–109). Coastal Research Library, Springer, Dordrecht.
- Mylroie, J.E., & Carew, J.L., (1990). The flank margin model for dissolution cave development in carbonate platforms. *Earth Surface Processes and Landforms*, 15, 413–424.
- Mylroie, J.E., & Carew, J.L., (1995a). Geology and karst geomorphology of San Salvador Island, Bahamas. *Carbonates and Evaporites*, 10, 193–206.
- Mylroie, J.E., & Carew, J.L., (1995b). Karst development on carbonate islands. In D. A. Budd, A. H. Saller, & P. M. Harris, (Eds.), *Unconformities and porosity in carbonate strata* (63). The American Association of Petroleum Geologists, Memoir.
- Mylroie, J. E., Carew, J. L., & Moore, A. I., (1995). Blue holes: Definitions and genesis. *Carbonates and Evaporites*, 10(2), 225–233.
- Mylroie, J. R., & Mylroie, J. E., (2007). Development of the carbonate island karst model. *Journal of Cave and Karst Studies*, 69, 59–75.
- Mylroie, J., & Mylroie, J., (2017a). Bahamian Flank Margin Caves as Hypogene Caves. In A. Klimchouk, A. Palmer, J. de Waele, A. Auler, P. Audra (Eds.), *Hypogene Karst Regions and Caves of the World. Cave and Karst Systems of the World* (757–758). Springer International Publishing.
- Mylroie, J., & Mylroie, J., (2017b). Role of karst denudation on the accurate assessment of glacial-eustasy and tectonic uplift on carbonate coast. *Geological Society, London, Special Publications*, 466, 171–185.
- Mylroie, J. E., Chak Ho, H., Infante, L. R., Kambesis, P., & Leist, J. W. (2016). Banana holes as syndepositional flank margin cave an advancing strandplain and their prediction using fuzzy-based spatial modelling. *The 16th Symposium on the Geology of Bahamas and other Carbonates Regions. Gerace Research Centre, San Salvador Bahamas*, 222–236.
- Mylroie, J., Lace, M., Albury, N., & Mylroie, J., (2020). Flank Margin Caves and the Position of Mid- to Late Pleistocene Sea Level in the Bahamas. *Journal of Coastal Research*, 36(2), 249–260.
- Palmer, A. N. (1991). Origin and morphology of limestone caves. *Geological Society of America Bulletin*, 103, 1–25.
- Paperless Cave Surveying (2017). DistoX2 Calibration Manual. <https://paperless.bheeb.ch/>.
- Purkis, S. J., & Harris, P. M., (2016). The extent and patterns of sediment filling of accommodation space on Great Bahama Bank. *Journal of Sedimentary Research*, 86, 294–310.
- Quintana Roo Speleological Survey, (QRSS), 2023, Quintana Roo Speleological survey, National Speleological Society. Available at <https://caves.org/project/qrss/> (Accessed 10 November 2023).
- Rodríguez, Castillo, J. F., Frausto, Martínez, O., Colín, Olivares, O., 2021, Morfometría de depresiones kársticas a escala detallada: El Cedral, Cozumel-México., 1990, Tropical and Subtropical Agroecosystems, 24(33), 1-14.
- Rosencrantz, E., 1990, Structure and tectonics of the Yucatán Basin, Caribbean Sea, as determined from seismic reflection studies. *Tectonics*, 9(5), 1037–1059.
- Roth, M. J., Mylroie, J. E., Mylroie, J. R, Ersek, V., Ersek, C. C., & Carew, J. L., (2006). Flank margin cave inventory of Bahamas. In *Proceedings of the 12th Symposium on the Geology of Bahamas and Other Carbonate Regions*, San Salvador, Bahamas, Gerace Research Center, 153–161.
- Schwabe, S. J., Carew, J. L., & Mylroie, J. E., (1993), The petrology of Bahamian Pleistocene eolianites and flank margin caves: Implications for Late Quaternary island development, in *Proceedings of the Sixth Symposium on the Geology of the Bahamas*. Porth Charlotte, Florida Bahamian Field Station, 149–164.
- Servicio Geológico Mexicano (SGM), 2006, Carta Geológico-Minera Cozumel F16-11, Quintana Roo y Yucatán. Servicio Geológico Mexicano [Map]. [http://mapserver.sgm.gob.mx/Cartas\\_Online/geologia/119\\_F16-8\\_GM.pdf](http://mapserver.sgm.gob.mx/Cartas_Online/geologia/119_F16-8_GM.pdf).
- Salgado-Garrido, H. E., Valera-Fernández, D., Trejo-Pelayo, S., Solleiro-Rebolledo, E., Barragan, R., Yáñez-Mendoza, G. Mejía-Ortiz, L., & López-Martínez, R., (2022). The microfacies distribution pattern of Cozumel Island in southeastern Mexico: An atoll-like model led by Quaternary glacioeustatic sea-level changes. *Journal of South American Earth Sciences*, 118, 103933. <https://doi.org/10.1016/j.jsames.2022.103933>
- Smart, P. L., Beddows, P. A., Doerr, S., Smith, L. S., & Whitaker, F., (2002). Hydrochemical processes and cave development on the Caribbean Coast, Yucatan Peninsula, Mexico, in J. B. Martin, C. M. Wicks, & I. D. Sasowsky (Eds.), *Hydrogeology and Biology of Post-Paleozoic Carbonate Aquifers* (7, 79–83). Karst Waters Institute Special Publication 7.
- Smart, P. L., Beddows, P. A., Coke, J., Doerr, S., Smith, S., & Whitaker, F. F., (2006). Cave development on the Caribbean coast of the Yucatan Peninsula, Quintana Roo, Mexico, in R. Harmon, & D. Wicks (Eds.), *Perspectives on Karst Geomorphology, Hydrology, and Geochemistry - A Tribute Volume to Derek C. Ford and William B. White* (404, 105–128). Geological Society of America Special Paper, 105–128.
- Stafford, K. W., Mylroie, J. E., Taborosi, D., Jenson, J. W., & Mylroie, J. R., (2005). Karst development on Tinian, Commonwealth of the Northern Mariana Islands: Controls on dissolution in relation to the carbonate island karst model. *Journal of Cave and Karst Studies*, 67 (1), 14–27.
- Szabo, B. J., Ward, W. C., Weidie, E., & Brady, M. J., (1978). Age and magnitude of the late Pleistocene sea-level rise on the eastern Yucatan Peninsula. *Geology*, 6, 713–715.
- Stoessell, R., Moore, Y. H., & Coke, J. G., (1993). The occurrence and effect of sulfate reduction and sulfide oxidation on coastal limestone dissolution in Yucatan cenotes. *Ground Water*, 31, 566–575.
- Thompson, W. G., Curran, H. A., Wilson, M. A., & White, B., (2011). Sea-level oscillations during the last interglacial recorded by Bahamas corals. *Nature Geoscience*, 4(10) 685–687. <https://doi.org/10.1038/ngeo1253>
- Uchupi, E., (1973) Eastern Yucatan continental margin and western Caribbean tectonics: Am. Assoc. Petrol. Geol. Bull. 57, 1075–1095.
- Vacher, H. L., (1988). Dupuit-Ghyben-Herzberg analysis of strip-island lenses. *Geological Society of America Bulletin*, 100, 580–591.
- Vacher, H. L., & Mylroie, J. E., (2002). Eogenetic karst from the perspective of an equivalent porous medium. *Carbonates and Evaporites*, 17, 182–196.
- van Hengstum, P. J., Scott, D. B., Gröcke, D. R., & Charette, M. A. (2011). Sea level controls sedimentation and environments in coastal caves and sinkholes. *Marine Geology*, 286, 35–50.
- van Hengstum, P. J., Richards, D. A., Onac, B. P., & Dorale, J. A., (2015). Coastal caves and sinkholes. In I. Shennan, A. J. Long, & B. P. Horton (Eds.), *Handbook of Sea-Level Research*. (pp. 83–103). John Wiley & Sons, Ltd, Chichester, UK.

- Valera-Fernández, D., Solleiro-Rebolledo, E., López-Martínez, R. A., Pi-Puig, T., Salgado-Garrido, H. E., & Cabada-Báez, H., (2020) Quaternary carbonates on the coast of Yucatan Peninsula and the island of Cozumel, México: Paleoenvironmental implications: *Journal of South American Earth Sciences*, 102, 102670. <https://doi.org/10.1016/j.jsames.2020.102670>
- Ward, W.C., (1997). Geology of coastal island northeastern Yucatan Peninsula perspective. In H. L. Vacher, & T.M. Quinn (Eds.), *Geology and Hydrogeology of carbonates islands* (275–298). Developments in Sedimentology.
- Ward, W. C., & Brady, M. J., (1979). Strandline sedimentation of carbonate grainstones, Yucatan Peninsula, Mexico. *American Association of Petroleum Geologist Bulletin*, 63, 362–369.
- de Waele, J. Plan, L., & Audra, P., (2009). Recent developments in surface and subsurface karst geomorphology: An introduction. *Geomorphology*, 106, 1–8.
- Waterstrat, W. J., Mylroie, J. E., Owen, M. A., & Mylroie, J. R., (2010) Coastal caves in Bahamian eolian calcarenites: differentiating between sea caves and flank margin caves using quantitative morphology. *Journal of Caves and Karst Studies*, 72(2), 61–74.
- Whitaker, F. F., & Smart, P. L., (1989,). Control on the rate and distribution of carbonate bedrock dissolution in the Bahamas. *Hydrology*, 84, 333–343.
-